J. Membrane Biol. 63, 165–190 (1981)

The Journal of
Membrane Biology

Interpretation of Current-Voltage Relationships for "Active" Ion Transport Systems: I. Steady-State Reaction-Kinetic Analysis of Class-I Mechanisms

Ulf-Peter Hansen*, Dietrich Gradmann**, Dale Sanders, and Clifford L. Slayman

Department of Physiology, Yale University School of Medicine, New Haven, Connecticut 06510

Summary. This paper develops a simple reaction-kinetic model to describe electrogenic pumping and co- (or counter-) transport of ions. It uses the standard steady-state approach for cyclic enzyme- or carrier-mediated transport, but does not assume rate-limitation by any particular reaction step. Voltage-dependence is introduced, after the suggestion of Läuger and Stark (*Biochim. Biophys. Acta* **211**:458–466, 1970), via a symmetric Eyring barrier, in which the charge-transit reaction constants are written as $k_{12}=k_{12}^o \exp(zF\Delta\Psi/2RT)$ and $k_{21}=k_{21}^o \exp(-zF\Delta\Psi/2RT)$. For interpretation of current-voltage relationships, all voltage-independent reaction steps are lumped together, so the model in its simplest form can be described as a pseudo-2-state model. It is characterized by the two voltage-dependent reaction constants, two lumped voltage-independent reaction constants (κ_{12}, κ_{21}), and two reserve factors (r_i, r_o) which formally take account of carrier states that are indistinguishable in the current-voltage (I-V) analysis. The model generates a wide range of I-V relationships, depending on the relative magnitudes of the four reaction constants, sufficient to describe essentially all I-V data now available on "active" ion-transport systems. Algebraic and numerical analysis of the reserve factors, by means of expanded pseudo-3-, 4-, and 5-state models, shows them to be bounded and not large for most combinations of reaction constants in the lumped pathway. The most important exception to this rule occurs when carrier decharging immediately follows charge transit of the membrane and is very fast relative to other constituent voltage-independent reactions. Such a circumstance generates kinetic equivalence of chemical and electrical gradients, thus providing a consistent definition of ion-motive forces (e.g., proton-motive force, PMF). With appropriate restrictions, it also yields both linear and log-linear relationships between net transport velocity and either membrane potential or PMF. The model thus accommodates many known properties of proton-transport systems, particularly as observed in "chemiosmotic" or energy-coupling membranes.

Key words: electrogenic pump, reduced kinetic model, Eyring barrier, current-voltage curve, ion-motive force, chemical rectification

Four different categories of concentrative or "active" transport systems have thus far been identified in biological membranes, classified on the basis of the manner in which metabolic energy is coupled to them. In the plasma membranes of nearly all animal, plant, and microbial cells, as well as in many subcellular organelles, are 1) ATP-driven ion pumps which reside in identifiable membrane ATPases (e.g., the Na^+-K^+ ATPase [27, 73, 83] and at least three distinct H^+-ATPases [5, 21, 28, 67, 74]), and 2) ion-gradient driven co- and countertransport systems for a variety of metabolic substrates (e.g., for sugars [18, 41, 44, 47, 48, 80, 91], amino acids [7, 18, 45, 80, 84], and nucleotide precursors [70]). In the membranes of many prokaryotes and the energy-coupling organelles of eukaryotic cells are 3) a variety of redox-driven ion (proton) transport systems [49, 90]; and in certain bacteria 4) sugar transport is driven *pari passu* by transphosphorylation, a process dubbed "group translocation" [75]. With some important exceptions (*see* e.g., Diamond [16], Sachs et al. [74]), the preponderance of transport systems in the first three categories are electrogenic; that is,

* *Current address:* Institut für Angewandte Physik, Universität Kiel, 2300 Kiel, West Germany.

** *Current address:* Max-Planck-Institut für Biochemie, 8033 Martinsried bei München, West Germany.

0022-2631/81/0063-0165 $05.20

they transfer electric charges through the membrane in which they reside.

In recent years, Mitchell's "Chemiosmotic Hypothesis" for photo- and oxidative phosphorylation has stimulated great interest in the chemistry of such charge transfer reactions in biological membranes, but the tools – both theoretical and experimental – for modeling charge flow within the framework of enzymatic reactions are only slowly becoming available. Except in the study of certain photo-redox reactions [40, 90], there has been a tendency to regard electrical events as epiphenomenological, rather than fundamental. An important manifestation of this idea has been the notion that passive channel structures mediate the transmembrane portion of pumped charge flow [69]. Morowitz [66], however, has pointed out that ordinary channels, by being purely dissipative, are not competent for such tasks as oxidative phosphorylation; accordingly, the putative channel proteins associated with some ion pumps [67] have been reinterpreted as ion-semiconductors. In the case of proton pumps, such proton semiconductors would transfer electrochemical energy through the membranes via shifting hydrogen bonds.

From a strictly kinetic point of view, also, it is clear that charge transfer reactions are central, rather than peripheral, to the underlying mechanisms. Essentially all transport processes can be represented as a cyclic series of reactions, in which membrane transit steps alternate in some fashion with membrane surface or interface (loading, unloading) reactions. To a first approximation, only the membrane transit steps should be sensitive to the transmembrane gradient of electric potential [56]. In other words, potential-dependent steps in the overall transport cycle are conceptually distinct from the steps of ion-binding or release and the steps of (for example) energizing transphosphorylation. (The latter, of course, may be influenced separately by membrane *surface* charge.)

Now, an exceedingly useful device for characterizing ordinary enzymatic reactions has been the steady-state velocity-concentration plot, in which the rate of appearance of product is displayed as a function of the reactant concentration. Following upon the early work of Wilbrandt and his collaborators [95], the same device has been applied to transport processes – active and passive – with considerable descriptive success, especially in those cases (e.g., the $Na^+ - K^+$ ATPase) where partial reaction chemistry has been accessible [23, 43, 73].

In the case of enzymes whose reaction product is electric current, a third dimension is added to the steady-state kinetic picture *viz.*, the electrical potential gradient or (in the simplest cases) the transmembrane difference of potential, universally called the "membrane potential." Since 1964, when Finkelstein [20] explicitly modeled active transport systems with a diffusion paradigm, numerous other attempts have been made to incorporate this third dimension into the overall kinetic description [e.g., 13, 24, 55, 57, 59]. But, quite apart from certain conceptual difficulties, most treatments have been limited by the problems of algebraic complexity inherent in any multiple-substrate enzymatic reaction. While it is clearly possible – given sufficient information or assumptions about underlying reaction constants – to calculate how reaction velocity (transport) *should* vary with substrate concentration or the membrane potential, the practical inverse problem, of estimating underlying reaction constants from measured velocities, potentials, and concentrations, has not been addressed.

A major purpose of the present paper, therefore, is to consider just what a careful steady-state kinetic description *can* reveal about underlying reaction constants for electrogenic "active" transport systems. In order to have a convenient handle, the term "carrier" will be used to refer to different forms of the transport system. That should not be taken literally, however. As in any kinetic description, it is the number of possible states and the arrangement of pathways between them, not the explicit physical interpretation, which characterizes the system. For the sake of simplicity, we will make two assumptions that are conventional in kinetic analyses of transport systems: a) that total carrier is conserved (fixed), and b) that all measurements are carried out under steady-state conditions. In addition, we shall restrict consideration c) to models having only a single pathway for flow of charge through the membrane; and we shall discuss d) variations of reaction velocity (current flow) as a function of membrane potential only, not of substrate concentration.

The effects of variable substrate concentration, multiple charge-flow pathways, and nonsteady-state conditions will be analyzed in subsequent papers. A restricted treatment of the consequences of variable substrate concentration, applied to chloride transport in giant algae, has recently been published [76]. A synopsis of results in the present paper with application to two specific electrogenic pumps, is being published in a symposium on Electrogenic Ion Pumps [32], and two preliminary reports have appeared [34, 51].

Definitions

Classes

In order to confine scope of the present paper within manageable limits, and, at the same time, to pro-

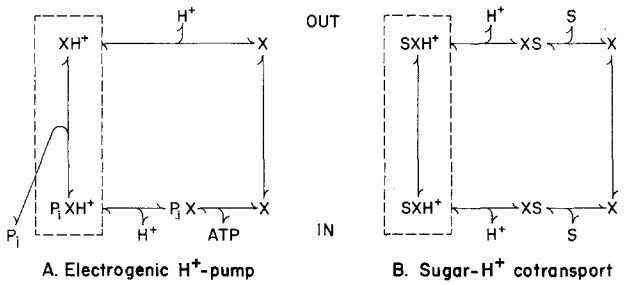

Fig. 1. Simplified reaction-sequence diagrams for electrogenic "active" transport systems. *A*. A reversible ATP-driven proton pump. *B*. A proton-coupled sugar cotransport system. Both diagrams are meant to be illustrative of kinetic models presently in use, but not necessarily realistic, either for the specific steps or the particular ion. Dashed boxes enclose the voltage-dependent reaction path

vide a framework for later generalization and expansion of the results, it is useful to classify ion transport models according to the number of distinct transmembrane pathways over which charge can be transferred. Class O models are those having no charge-transfer steps, and would describe such transport processes as neutral $Na^+ - Cl^-$ cotransport in gall bladder [16], and perhaps the emerging $K^+ - Na^+ - 2Cl^-$ cotransport by erythrocyte and cultured-cell membranes [25, 50, 77]. Class I models are those having a single charge-transfer step, and have been applied to a number of familiar transport processes, two of which are diagrammed in simple form in Fig. 1: *A*) pumped proton extrusion by various microorganisms and plants [7, 28, 84], and *B*) H^+-sugar cotransport or Na^+-sugar cotransport in a large variety of membranes [18, 41, 42, 44, 47, 48]. In both of the models shown, there is only a single pathway (enclosed in the dashed rectangle) for charge to cross the membrane, and we assume this pathway alone is voltage-sensitive [56]. All other steps take place as scalar chemical reactions in the membrane-solution interfaces or as transit through the membrane by electrically neutral species (in these models, unbound carrier).

Class II models are those with two distinct charge transport limbs, as must be postulated minimally for the sodium pump ($Na^+ - K^+$ ATPase) of animal-cell membranes [43], for $Na^+ - Ca^{++}$ exchange transport seen in nerve membranes [71], and for $Na^+ - H^+$ or $K^+ - H^+$ exchange transport observed in bacteria [6, 10, 68, 78] and in renal tubules [47]. [It should be noted that Class II models (more generally, Class-Even models) *need* not be electrogenic overall during steady-state operations; but even then individual reaction rate constants and the overall cycle rate can be voltage sensitive.] Class III, Class IV, or higher models might seem superfluous at the present time, but their existence has in fact already been postulated, to account for *electrogenic* $K^+ - H^+$ exchange through lipid films, mediated by nigericin [60]; they should also perhaps be considered in connection with multi-ion exchange mechanisms observed under osmotic stress in erythrocyte and cultured-cell membranes [25, 50, 77] and under pH stress in various excitable membranes [93, 94].

Carrier States

Within any one class, models which attempt to be physically realistic are likely to incorporate many distinct forms, or states, of the carrier. For the best-described simple carrier system, the valinomycin-K^+ system, relaxation kinetic data support the existence of at least four states: loaded, unloaded, located at the membrane inside surface, and located at the membrane outside surface [56, 87, 88]. For the best understood active transport system, the $Na^+ - K^+$ pump, a minimum of eight different states of the carrier seem to be required [43, 73], and most ion-coupled cotransport systems seem to demand at least six different carrier states [24, 48, 76]. Of course, the actual number of physically distinct carrier states is not known with certainty for any transport system, which means that any particular model, envisioned with m distinct states of the carrier, is most appropriately referred to as a *pseudo-m-state* model. The term *n-state model* will be reserved for all "real" models.

In order to simplify the computational notation, subscripting numbers will be attached to the states of any m-state Class I model, according to the convention illustrated in Fig. 2: odd subscripts for carrier states located at the membrane inside surface, even subscripts for carrier states located at the membrane outside surface. For Class I models, numbering should begin with the charge-sensitive carrier forms as states 1 and 2, keeping the subscript numbers in register across the membrane, as far as possible. Apparent reaction constants will be designated with the corresponding state subscripts (e.g., k_{12} for the transition *from* state N_1^+ *to* state N_2^+) and will contain, throughout this discussion, the actual chemical concentrations of nonenzyme reagents (i.e., k_{21} contains $[P_i]$, k_{31} contains $[H^+]_i$, etc.).

Reduction of Models

Every Class I n-State Model Can Be Reduced to a 2-State Model, with respect to measurement of the steady-state membrane currents or the corresponding chemical net fluxes. In other words, for purposes of current-voltage (*I-V*) analysis, all Class I models, including those of Figs. 1 and 2, can be compressed into that of Fig. 3, which, in keeping with the de-

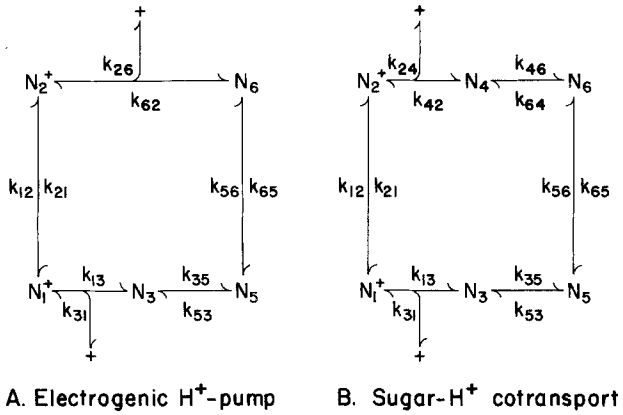

Fig. 2. Transcription of the diagrams of Fig. 1, to define the apparent reaction constants. Terms for membrane potential and for concentrations of the chemical ligands are subsumed within the reaction constants. Thus, for example, k_{53} could be written as $k'_{53}[ATP]$, in part *A*; and as $k'_{53}[S]$, in part *B*. The following conventions are used for designating carrier states: odd subscripts = carrier states associated with membrane inside surface; even subscripts = carrier states associated with membrane outside surface; superscript + or − indicate charged forms of the carrier; missing carrier states (e.g., N_4 in *A*) call attention to reaction asymmetry

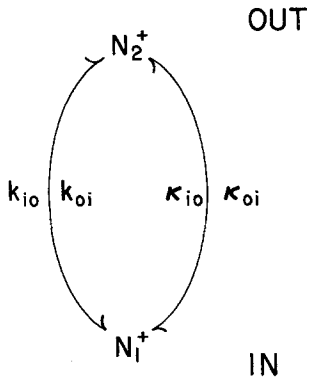

Fig. 3. Reduction of the diagrams of Figs. 1 and 2 to the pseudo-2-state model. All carrier states and reaction constants lying to the right of the charge-transit step are assumed to be voltage-independent and are combined into the lumped reaction constants κ_{io} and κ_{oi}. In the text, k_{io}, k_{oi}, κ_{io}, and κ_{oi} are referred to as *empirical* reaction constants

finitions above, we shall call the pseudo-2-state model.

Reduction comes about fundamentally for two reasons: 1) the transport current or net ion flux depends only upon the difference between N_1^+ and N_2^+, and 2) *under steady-state conditions* all of the voltage-independent states of the carrier can be expressed as functions of N_1^+, N_2^+, and various algebraic combinations of the intermediate reaction constants, without additional information. The first point is obvious, and can be written formally as

$$i(\text{current}) = zF(k_{12}N_1^+ - k_{21}N_2^+), \tag{1}$$

for all Class I models (z is the transport stoichiometry, or number of charges carried per turn of the cycle; F is the Faraday constant). The second point is not so obvious, but emerges when the voltage-independent reactions are considered to form a chain delimited by the "beginning" and "end" states N_2^+ and N_1^+. Then, provided the intermediate reaction constants do not change (which means that $[H^+]_i$, $[P_i]$, etc., must remain fixed) during changes of membrane potential, we can write for each intermediate state N_j ($j = 3, 4, 5, 6, \ldots, n$)

$$N_j = r_{j1}N_1^+ + r_{j2}N_2^+ \tag{2}$$

in which r_{j1} and r_{j2} are algebraic combinations of the voltage-independent reaction constants, as referred to above. The explicit evaluation of r_{j1} and r_{j2} depends, of course, on the nature of each particular "real" n-state model.

Since total carrier (N) is just

$$N = \sum_{j=1}^{n} N_j \tag{3}$$

Eq. (2) further implies that N can also be expressed as a function of N_2^+ and N_1^+. Specifically, by combining Eqs. (2) and (3), plus the identities $r_{11} = 1 = r_{22}$ and $r_{12} = 0 = r_{21}$, we obtain

$$N = \sum_{j=1}^{n} r_{j1}N_1^+ + \sum_{j=1}^{n} r_{j2}N_2^+ \quad \text{or} \quad N = r_i N_1^+ + r_o N_2^+. \tag{4a, b}$$

In the right-hand form, the terms

$$r_i = \sum_{j=1}^{n} r_{j1} \quad \text{and} \quad r_o = \sum_{j=1}^{n} r_{j2} \tag{5a, b}$$

will be called *reserve* factors. They – or, to be exact $(r_i - 1)$ and $(r_o - 1)$ – specify the amount of carrier which is sequestered in the voltage-independent reactions. This meaning can be seen more clearly by comparing Eq. (4) with the corresponding relationship for a "real" 2-state model: in that case, total carrier would be simply the sum of N_1^+ and N_2^+.

Formal Role of Reserve Factors in the Pseudo-2-State Model

The manner in which the reserve factors actually enter the reaction constants of the pseudo-2-state model can be seen by deriving the expression for transport current with, and without, explicitly in-

cluding r_i and r_o. The conventional starting point for such derivations is to write the ensemble of steady-state mass equations for different carrier states. For the 2-state model these are simply

$$-\frac{dN_1^+}{dt}=0=(k_{12}+\kappa_{12})\,N_1^+-(k_{21}+\kappa_{21})\,N_2^+ \tag{6}$$

and

$$N=r_i N_1^+ + r_o N_2^+ \tag{4b}$$

where the subscripts 12 and 21 are used to distinguish that case in which the reserve factors are to be explicitly included. Eqs. (4b) and (6) can be solved simultaneously, to give the following expressions for N_1^+ and N_2^+, in terms of the total carrier N:

$$N_1^+=\frac{k_{21}+\kappa_{21}}{r_i(k_{21}+\kappa_{21})+r_o(k_{12}+\kappa_{12})}N \tag{7a}$$

and

$$N_2^+=\frac{k_{12}+\kappa_{12}}{r_i(k_{21}+\kappa_{21})+r_o(k_{12}+\kappa_{12})}N, \tag{7b}$$

and these values are then inserted into Eq. (1) to get the transport current which, after collecting terms and multiplying both denominator and numerator by $r_i r_o$, becomes

$$i=zF\frac{N}{r_i r_o}\frac{r_i\kappa_{21}\cdot r_o k_{12}-r_o\kappa_{12}\cdot r_i k_{21}}{r_o k_{12}+r_i k_{21}+r_o\kappa_{12}+r_i\kappa_{21}}. \tag{8}$$

The corresponding result without explicit inclusion of the reserve factors is just

$$i=zF\bar{N}\frac{\kappa_{oi}k_{io}-\kappa_{io}k_{oi}}{k_{io}+k_{oi}+\kappa_{io}+\kappa_{oi}} \tag{9}$$

where $\bar{N}$ and the subscripts io and oi designate parameters with concealed reserve factors (Fig. 3). Comparing Eqs. (8) and (9), we can write

$$k_{12}=\frac{k_{io}}{r_o},\quad k_{21}=\frac{k_{oi}}{r_i},\quad \kappa_{12}=\frac{\kappa_{io}}{r_o},\quad \kappa_{21}=\frac{\kappa_{oi}}{r_i}. \tag{10a-d}$$

Thus, the normal application of Fig. 3 [Eq. (9)] to *I-V* data for Class-I systems will yield empirical reaction constants which must be divided by the appropriate reserve factors in order to get realistic values. This is only a minor complication for κ_{io} and κ_{oi}, since they are already complex. The corresponding result for total carrier ($N=r_i r_o \bar{N}$) is also unimportant, since that parameter normally acts as a scaling factor. However, the result for k_{io} and k_{oi} can be very significant, since it means that the voltage-dependent reaction constants are distorted by concealment of carrier in the voltage-independent pathway. The evaluation of r_i and r_o, along with some of their fundamental properties, will be discussed below (*see* Usefulness and Meaning ..., Appendix I, and Appendix II).

Voltage-Dependence

The voltage-dependence implied by Eq. (9) remains to be specified. In the absence of detailed knowledge of the electrical profile across the membrane, the manner of introducing voltage-dependence must be somewhat arbitrary. While some authors [59] have adopted the constant-field formulation, we prefer the approach of Läuger and Stark [56], who introduced the symmetric Eyring barrier, so that

$$k_{io}=k_{io}^o\exp(zu/2)\quad\text{and}\quad k_{oi}=k_{oi}^o\exp(-zu/2). \tag{11a,b}$$

Here, k_{io}^o and k_{oi}^o represent voltage-independent constants, whose values are defined at zero membrane potential; and u, the reduced voltage, is

$$u=F\Delta\psi/RT, \tag{12}$$

where R, T, and F have their usual meaning, z is the valence of the charged particle crossing the membrane, and $\Delta\psi$ is the membrane potential. Apart from the simplicity and aesthetic appeal of this approach, it has the advantage of being formally equivalent to defining carrier states N_1^+ and N_2^+ as *electro*chemical activities (taking zero potential at the center of the membrane), whenever the voltage-dependent pathway is traversed. (This equivalence arises because only the products $k_{io}N_1^+$ and $k_{oi}N_2^+$ are used [by analogy with Eq. (6)] to commence the derivation of Eq. (9).)

Incorporating Eqs. (11) into Eq. (9). and compressing the scaling factor ($N^*=zF\bar{N}$), gives

$$i=N^*\frac{\kappa_{oi}k_{io}^o\exp(zu/2)-\kappa_{io}k_{oi}^o\exp(-zu/2)}{k_{io}^o\exp(zu/2)+k_{oi}^o\exp(-zu/2)+\kappa_{io}+\kappa_{oi}}, \tag{13}$$

for the generalized current-voltage relationship of Class I electrogenic ion transport systems. (In this formulation, current is taken to be positive for outward movement of positive charge, according to the usual electrophysiological convention.)

It is evident, particularly from Eqs. (4) and (8), that the above *I-V* relationship must *conceal* the majority of parameters for the n-state transport system. Fortunately, however, examination of limiting conditions and special cases, along with study of localized drug effects, can extract very considerable

information from Eq. (13); and such techniques underlie the remaining sections of this paper.

Geometric Properties of Class I Current-Voltage Curves

Elementary Parameters

Simple inspection of Fig. 3 and Eqs. (12) and (13) reveals several important facts. Current saturates as a function of membrane potential, at extreme positive or negative potentials, and the *saturating currents* characterize the voltage-independent reaction constants in the pseudo-2-state model:

$$i_{sat+} = N^* \kappa_{oi} \quad \text{and} \quad i_{sat-} = -N^* \kappa_{io}. \tag{14a, b}$$

Current flow stops ($i=0$) when $\exp(z u) = \kappa_{io} k^o_{oi} / \kappa_{oi} k^o_{io}$, which defines the *reversal potential* (E_r) of the transport system as

$$E_r = \frac{RT}{zF} \ln \frac{k^o_{oi}}{k^o_{io}} \cdot \frac{\kappa_{io}}{\kappa_{oi}}, \tag{15}$$

within which equilibrium potentials for the charge-carrying (E_c) and neutral (E_n) pathways can also be defined:

$$E_c = \frac{RT}{zF} \ln \frac{k^o_{oi}}{k^o_{io}} \quad \text{and} \quad E_n = \frac{RT}{F} \ln \frac{\kappa_{io}}{\kappa_{oi}}. \tag{16a, b}$$

The sum $E_c + E_n/z$ gives E_r. Finally, the *short-circuit current* (i_{sc}) is given by

$$i_{sc} = N^* \frac{\kappa_{oi} k^o_{io} - \kappa_{io} k^o_{oi}}{k^o_{io} + k^o_{oi} + \kappa_{io} + \kappa_{oi}}. \tag{17}$$

The four relationships stated in Eqs. (14), (15) and (17), whose values can be measured on a complete *I-V* curve, allow straightforward calculation of all four empirical reaction constants. [The stoichiometric coefficient (z) must be assumed (but *see* the section *Slope and Spread*, below); and each empirical constant contains the scaling factor N^*.] Explicitly, κ_{oi} and κ_{io} are given by slight rearrangement of Eqs. (14a) and (14b). k^o_{io} and k^o_{oi} can be obtained by simultaneous solution of Eqs. (15) and (17). This operation is facilitated by writing the "reduced" reversal potential, by analogy with Eq. (12):

$$u_r = FE_r/RT. \tag{18}$$

After considerable algebra, and substitution of Eqs. (14) for κ_{io} and κ_{oi},

$$k_{io} = \frac{1}{N^*} \cdot \frac{i_{sc}(i_{sat+} - i_{sat-})}{i_{sat+}(1 - \exp(z u_r)) - i_{sc}\left(1 - \frac{i_{sat+}}{i_{sat-}} \exp(z u_r)\right)}, \tag{19}$$

and

$$k_{oi} = \frac{1}{N^*} \cdot \frac{i_{sc}(i_{sat+} - i_{sat-})}{i_{sat-}(1 - \exp(-z u_r)) - i_{sc}\left(1 - \frac{i_{sat-}}{i_{sat+}} \exp(-z u_r)\right)}. \tag{20}$$

Symmetry

The basic shape of the Class I current-voltage relationship, and its diagnostic features, become clearest if the coordinate system is first shifted so the origin coincides with the point defined by $\Delta\psi = E_c$ and $i =$ the *mid-range current* (i_{mid}):

$$i_{mid} = \tfrac{1}{2}(i_{sat+} + i_{sat-}) = \frac{N^*}{2}(\kappa_{oi} - \kappa_{io}). \tag{21}$$

In order to make the appropriate axial translation, we define new current ($\imath$) and voltage (v) variables, such that

$$i = \imath + \frac{N^*}{2}(\kappa_{oi} - \kappa_{io}) \quad \text{and} \quad u = v + \frac{zF}{RT} E_c. \tag{22a, b}$$

These are inserted into Eq. (13), which can be rearranged to give $\imath$ strictly as a function of v. By substituting the identity $\exp(zFE_c/2RT) = \sqrt{k^o_{oi}/k^o_{io}}$, an equation is obtained in which the expression $\sqrt{k^o_{oi} k^o_{io}}$ appears as the coefficient of all the exponential terms; after both numerator and denominator are divided by $\sqrt{k^o_{oi} k^o_{io}}$, the following *I-V* equation is obtained:

$$\imath = N^* \frac{\kappa_{io} + \kappa_{oi}}{2} \cdot \frac{\frac{\kappa_{io} - \kappa_{oi}}{\sqrt{k^o_{oi} k^o_{io}}} + \exp\left(\frac{zv}{2}\right) - \exp\left(-\frac{zv}{2}\right)}{\frac{\kappa_{io} + \kappa_{oi}}{\sqrt{k^o_{oi} k^o_{io}}} + \exp\left(\frac{zv}{2}\right) + \exp\left(-\frac{zv}{2}\right)}. \tag{23}$$

While this result as such may not seem clearer than Eq. (13), it readily splits into two superposable currents, which we can call "even" and "odd", because of the curve shapes they represent. Letting S^*,

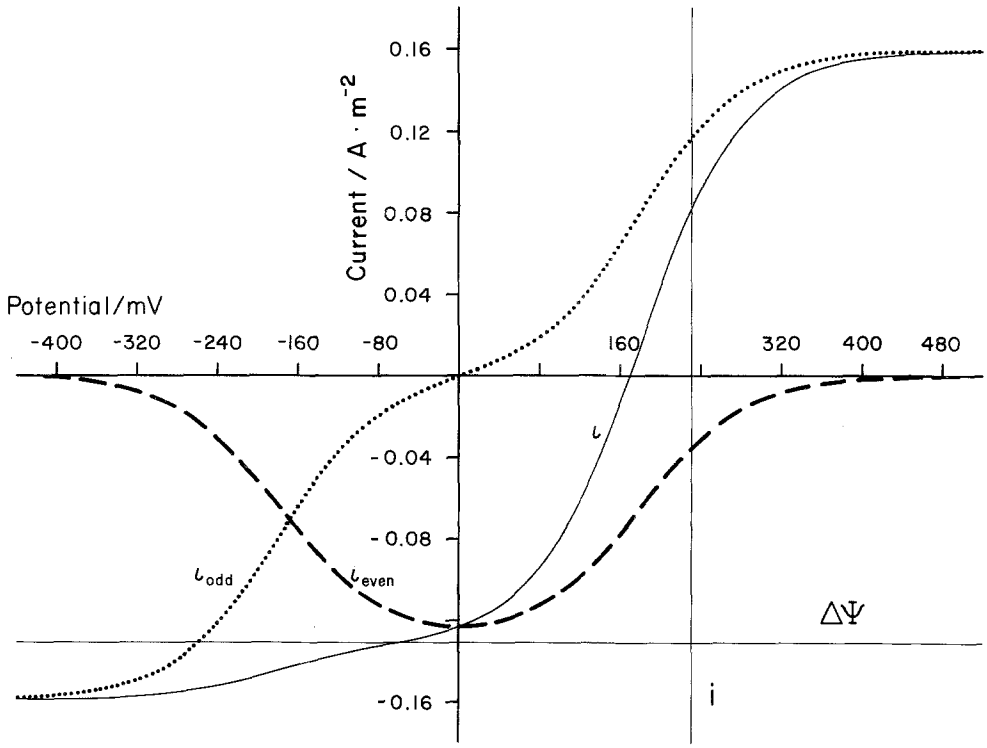

Fig. 4. Demonstration of the symmetric behavior of the pseudo-2-state model, plotted on current-voltage (*I-V*) axes. The following values were used for terms in Eq. (13): $N=10^{-8}$ moles/cm^2, $k^o_{io}=10^3$/sec, $k^o_{oi}=10^{-1}$/sec, $\kappa_{oi}=300$/sec, $\kappa_{io}=30$/sec, giving a reversal potential E_r (Eq. (15)) of −296 mV. The primary coordinate system is shown by the light lines designated i and $\Delta\psi$. A secondary coordinate system, which brings out the symmetry, is shown by darker lines, for which the voltage coordinate is $v=\Delta\psi-E_c=\Delta\psi-236$ mV [*see* Eq. (16a)], and the current coordinate is $\iota=i-i_{mid}$. In these coordinates, ι is given by Eq. (23), ι_{even} by Eq. (25a), and ι_{odd} by Eq. (25b)

the *saturation factor*, be

$$S^*=\frac{N^*}{2}(\kappa_{io}+\kappa_{oi}), \tag{24}$$

gives

$$\iota_{\text{even}}=S^*\frac{\dfrac{\kappa_{io}-\kappa_{oi}}{\sqrt{k^o_{oi}k^o_{io}}}}{\dfrac{\kappa_{io}+\kappa_{oi}}{\sqrt{k^o_{oi}k^o_{io}}}+\exp\left(\dfrac{z\,v}{2}\right)+\exp\left(-\dfrac{z\,v}{2}\right)} \tag{25a}$$

and

$$\iota_{\text{odd}}=S^*\frac{\exp\left(\dfrac{z\,v}{2}\right)-\exp\left(-\dfrac{z\,v}{2}\right)}{\dfrac{\kappa_{io}+\kappa_{oi}}{\sqrt{k^o_{oi}k^o_{io}}}+\exp\left(\dfrac{z\,v}{2}\right)+\exp\left(-\dfrac{z\,v}{2}\right)}. \tag{25b}$$

These functions are plotted in Fig. 4, for an arbitrary set of parameters (detailed in the Figure legend). Several properties are now apparent. First, the overall *I-V* relationship ($\iota=\iota_{\text{even}}+\iota_{\text{odd}}$) is not symmetric in general. It can become symmetric, however, under two conditions: a) when $\sqrt{k^o_{oi}k^o_{io}}\gg(\kappa_{io}+\kappa_{oi})$, which means that carrier reloading (*see* Fig. 3) is slow; and b) when the mid-range current is zero ($\kappa_{oi}=\kappa_{io}$). In both of these cases ι_{even} becomes zero.

The former case is particularly interesting, since then the *I-V* curve is simply a hyperbolic tangent function of voltage:

$$\iota=\iota_{\text{odd}}=S^*\tanh\left(\frac{z\,v}{2}\right). \tag{26}$$

This case is drawn as curves (*C* and *D*) in Fig. 5, and will be discussed in more detail below. Fig. 4 and Eqs. (25) show that the shape of the overall *I-V* curve depends both upon the relative contribution of ι_{even} and ι_{odd} (which means the ratio $(\kappa_{io}-\kappa_{oi})/\sqrt{k^o_{oi}k^o_{io}}$) and upon the relative contribution of the voltage-independent term in both denominators: $(\kappa_{io}+\kappa_{oi})/\sqrt{k^o_{oi}k^o_{io}}$. Several cases are drawn in Fig. 5; observed *I-V* plots closely resembling any of these curves could be taken as diagnostic for the relative magnitude of the reaction constants in the pseudo-2-state model.

Slope and Spread

When *I-V* data can in fact be well-described by the hyperbolic tangent function (Fig. 5, curves *C* or *D*)

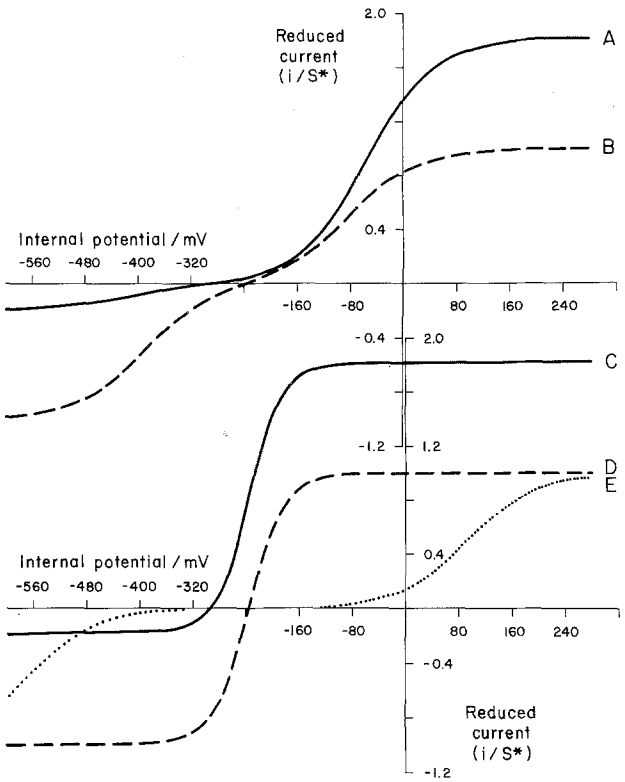

Fig. 5. Selected current-voltage curves calculated from the pseudo-2-state model [Eq. (13)], but plotted on a "reduced" current axis, which is normalized for the scaling factors and maximal current span. $S^* = zFN(\kappa_{oi}+\kappa_{io})/2r_i r_o$ [*see* Eqs. (8), (9), (13), and (24)]. The following empirical reaction constants were used (units of sec^{-1}):

	Voltage-dependent		Voltage-independent		
	k^o_{io}	k^o_{oi}	κ_{oi}	κ_{io}	E_r (mV)
A	1000	0.1	300	30	−296
B	1000	0.1	100	100	−236
C	1000	0.1	0.03	0.003	−296
D	1000	0.1	0.03	0.03	−236
C	10	0.001	30	30	−236

Curve *A* is the same as that drawn in Fig. 4. Note that when the voltage-dependent reaction constants are large with respect to the voltage-independent constants, the curves (*C*, *D*) resemble a hyperbolic tangent function [*see* Eq. (26)]. When the voltage-independent constants are unequal (curves *A*, *C*), the membrane potential drives a large saturating current in one direction (here, upward, in the manner of an ion pump), but only a small current in the other direction (here, downward, in the manner for ATP synthesis or cosubstrate accumulation). When the voltage-dependent reaction constants are small (curve *E*), two regions of voltage-dependent current flow separate three regions of voltage-independent current flow. Curve *B* shows an intermediate case

several other useful statements emerge from Eq. (26). Since $d(zv/2)/d\Delta\psi = d(zu/2)/d\Delta\psi = zF/2RT$, the slope conductance at limiting steepness ($v \to 0$, or $\Delta\psi \to E_c$) is just the product of $zF/2RT$ and the saturation factor:

$$\left.\frac{di}{d\Delta\psi}\right]_{\Delta\psi = E_c} = S^* \frac{zF}{2RT}. \tag{27}$$

For a transport stoichiometry of $z=1$ charge/cycle, the slope conductance would be S^* per 51 mV. S^* is normally obtained by fitting *I-V* data directly to the hyperbolic tangent function, or by scaling the span between i_{sat+} and i_{sat-}; subsequent calculation of the expected slope conductance, *via* Eq. (27), can then act as a test for consistency. There are three possible outcomes. If the conductance approximates S^* per 51 mV, Eq. (26) is verified, and $\sqrt{k^o_{oi}k^o_{io}} \gg (\kappa_{io}+\kappa_{oi})$, although the fact that only the ratio k^o_{oi}/k^o_{io} appears (in E_c) in Eq. (26) implies that the individual values of these two reaction constants cannot be obtained. If conductance is appreciably less than S^* per 51 mV, Eq. (26) is incorrect, and probably $\sqrt{k^o_{oi}k^o_{io}} \not\gg (\kappa_{io}+\kappa_{oi})$, which would mean that carrier reloading through the voltage-insensitive steps is not rate-limiting. And if conductance is significantly greater than S^* per 51 mV, a stoichiometry greater than 1:1 must be assumed.

Also characteristic is the voltage displacement $(\Delta\psi - E_c)$ that is required to yield half the saturating current. In that case, $\tanh(zv/2)=0.5$, and $\operatorname{arctanh}(0.5)=zv/2=0.549$, from which follows

$$\Delta\psi - E_c = 28/z \quad \text{(in mV)}. \tag{28}$$

Usefulness and Meaning of Reserve Factors Interpretation Based on 3-State and 4-State Models

A difficult problem underlying kinetic modeling of real enzymatic processes, and of transport processes in particular, is the likelihood that the "real" reaction cycle will contain one or more unidentified states. Reaction constants obtained from kinetic analysis, then, are likely to be physically complex (i.e., they are pseudo reaction constants) and not subject to simple interpretation or assignment. Each time a model is "upgraded" to take account of new data, or data of a new type, all terms in the model must be reevaluated. This tends to reduce the process of kinetic modeling to one of purely empirical curve-fitting. Traditionally, two major techniques have been used in order to focus the physical interpretation of the constants in kinetic models: partial reaction analysis, and relaxation analysis. The former, involving either blockade or bypassing of

specified segments in the overall cycle, has been most useful for complex biological transport processes, such as oxidative phosphorylation [9] or ATP-driven Na^+/K^+ pumping [23, 43]. The latter, involving sudden steps in driving force, has been applied principally to the nerve action potential and to simple nonbiological transport processes created in lipid bilayer membranes [56, 87, 88].

In most *I-V* analyses on biological systems, however, it happens both that extensive experimental manipulation of this sort is not feasible and that the accessible segments of *I-V* curves are too short or too nearly linear for even the four empirical reaction constants to be evaluated securely from a single *I-V* plot. In such circumstances, reserve factors provide a means for evaluating, or at least limiting, the probable effects of hidden reaction steps. The approach is particularly useful when combined with treatment by drugs[1] or other experimental changes which can be supposed to modify a single step in the overall cycle, since the finite reaction time for any such change permits generation of a set of *I-V* curves (progressing from zero drug-effect to full drug-effect) in which all kinetic parameters except one are held in common, and that one must change systematically with time. Depending upon whether the particular change *in fact* acts on a step immediately adjacent to the voltage-dependent reaction, or acts some distance away, the pseudo-2-state model can be expanded into a pseudo-3-state or pseudo-4-state kinetic model.

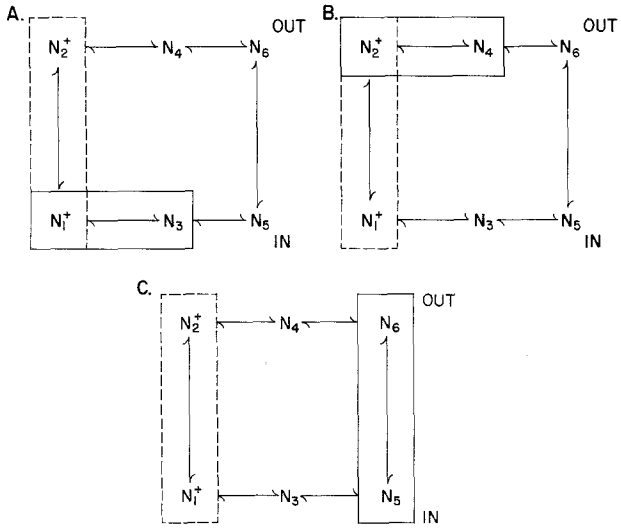

Fig. 6. Diagram of a generalized 6-state transport model designating three ways to exclude an experimentally manipulated reaction step from the lumped set of voltage-independent reactions. As in Fig. 1, the dashed rectangles enclose the voltage-dependent path; the solid rectangles designate voltage-independent step to be excluded from the lump. The excluded step might be manipulated by changing the ionic composition of the cytoplasm (*A*) or the medium (*B*) (i.e., pH in Fig. 1*A*); by varying internal or external cosubstrate levels (as in Fig. 1*B*), or the ATP concentration (Fig. 1*A*); or it might be manipulated by use of site-specific inhibitors. For convenience, all of these possible treatments are referred to in the text as "drugs" (*see* Footnote 1). The crucial difference between *C* and *A* or *B* is that in *C* the step to be manipulated, and therefore excluded from the lumping procedure, is *not adjacent* to the voltage-dependent reaction step. For *A* and *B* pseudo-3-state kinetic models can be used, but for *C* a pseudo-4-state model is required, because there are two separate lumps: $N_2^+ \leftrightharpoons N_6$, $N_1^+ \leftrightharpoons N_5$

Development of Pseudo-3- and Pseudo-4-State Models

In combining drug experiments with current-voltage analysis, we apply the same rationale to the development of kinetic models as was used for *I-V* analysis alone: to represent a real *n*-state process, select the pseudo-*m*-state model having the smallest number of states which will allow all reactions that undergo change during the experiment to be *excluded* from the lumping procedure. Thus, for *I-V* analysis alone a pseudo-2-state model is sufficient, because only the transmembrane movement of charge, with rate constants k_{12} and k_{21} (Fig. 2) is voltage dependent; all other reactions can be represented by the lumped reaction constants κ. For a drug acting at a single reaction step, a 3-state model is sufficient if the affected step is immediately adjacent to the voltage-dependent reaction (counterclockwise or clockwise); and a 4-state model is sufficient if the affected step is distant on both sides from the voltage-dependent reaction.

The three possibilities are diagrammed in Fig. 6, using a simplified version of the 6-state model in Fig. 2*B* as the frame of reference. As in Fig. 1, dashed rectangles delimit the voltage-dependent reactions; and the solid rectangles delimit the additional reaction to be excluded from the lumping procedure. The corresponding 3- and 4-state models are displayed in Fig. 7, where *s* now designates the excluded reaction constants. Mathematical development of the 3- and 4-state models is detailed in Appendix I; some rules for the behavior of r_i and r_o, plus some computations of values, are given in Appendix II; and a synopsis of equivalences for r_i, r_o, κ_{12}, κ_{21}, κ_{io}, and κ_{oi} is listed in Table 1. When reserve factors and lumped reaction constants are evaluated in terms of these models, three modes of kinetic influence on the empirical (2-state) reaction constants can be identified, according to the locus, direction, and sign of the *apparent* change.

[1] The term "drug" is used here in a very general sense, to mean any chemical or physical agent or maneuver which selectively modifies some step in the transport cycle. By such a definition changes of substrate level might be called drugs, and, indeed, other authors have made extensive use of substrate variations to study the interrelation of voltage-dependent and voltage-independent steps in ion transport systems [24, 35].

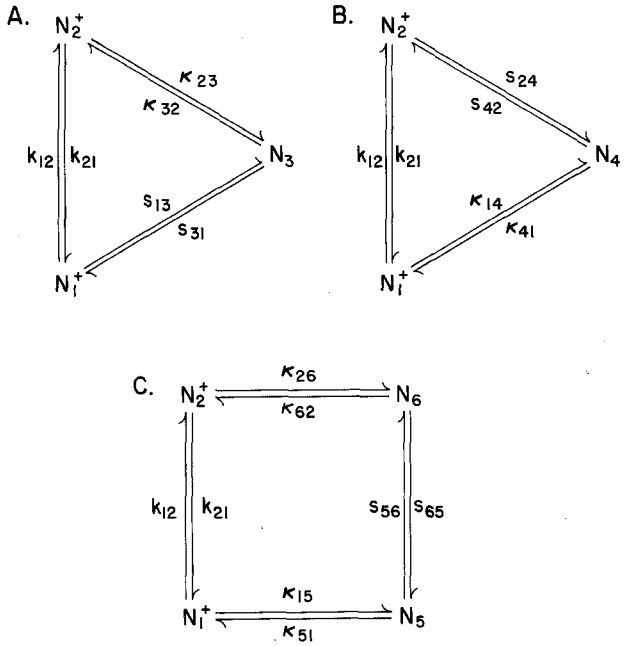

Fig. 7. Reduction of the diagram of Fig. 6 to the pseudo-3-state model (*A, B*), and the pseudo-4-state model (*C*). k designates the voltage-dependent path; κ, the lumped reaction steps; and s, the step to be manipulated experimentally and to be excluded from the lumping procedure

Consequences of Modifying a Dominant Rate-Limiting Reaction

The simplest behavior of the reserve factors and the least distortion of the empirical reaction constants defined by Eqs. (8)–(10) occurs when one reaction step in the voltage-independent pathway is much slower than the others. The reserve factors, r_i and r_o, are independent of such a slow reaction step, and a drug acting on that step cannot influence the empirical rate constants, k_{oi}^o and k_{io}^o, for the voltage-dependent step. The verbal argument is exactly the same whether the rate-limiting reaction is immediately adjacent to the voltage-dependent step or is separated from it by faster reactions. This means that either the pseudo-3-state model or the pseudo-4-state model can be used for the formal description; but since the 4-state model yields equations that are simpler (because of symmetry), we shall develop the result only for that model.

In Fig. 7*C*, let the reaction constants s_{56}, $s_{65} \ll \kappa_{26}$, κ_{62}, κ_{15}, κ_{51}. Then the right-hand column of Table 1 yields

$$r_i = r_1 + r_5 \frac{\kappa_{15}}{\kappa_{51}} \quad \text{and} \quad r_o = r_2 + r_6 \frac{\kappa_{26}}{\kappa_{62}}, \tag{29a, b}$$

and

$$\kappa_{12} = s_{56} \frac{\kappa_{15}}{\kappa_{51}} \quad \text{and} \quad \kappa_{21} = s_{65} \frac{\kappa_{26}}{\kappa_{62}}, \tag{30a, b}$$

in which $r_x (x = 1, 2, 5, 6)$ are the 4-state reserve factors [*see* Appendix I, Eq. (A4-5b)]. Since r_i, r_o, and r_x are by definition independent of s_{56} and s_{65}, it is clear that the empirical voltage-dependent reaction constants, $k_{io} (= r_o k_{12})$ and $k_{oi} (= r_i k_{21})$, are also independent of s_{56} and s_{65}. Therefore, the only kinetic effect which the slow reaction can have is upon the empirical voltage-independent constants, $\kappa_{io} (= r_o \kappa_{12})$ and $\kappa_{oi} (= r_i \kappa_{21})$.

There are two important consequences of this circumstance. First, the distortion of k_{io} and k_{oi} due to reactions concealed in the 2-state model is *static*,

Table 1. Interpretation of (2-state) reserve factors and reaction constants by means of the pseudo-3-state and pseudo-4-state models

	2-State (empirical form)	2-State (explicit form)	3-State	4-State	Equation Nos.
Voltage-sensitive reaction constants	$k_{io} = r_o k_{12}$	$k_{12} =$	k_{12}	k_{12}	(10a)
	$k_{oi} = r_i k_{21}$	$k_{21} =$	k_{21}	k_{21}	(10b)
Voltage-insensitive reaction constants	$\kappa_{io} = r_o \kappa_{12}$	$\kappa_{12} =$	$\frac{\kappa_{32} s_{13}}{s_{31} + \kappa_{32}}$	$\frac{s_{56} \kappa_{15} \kappa_{62}}{(s_{56} + \kappa_{51})(s_{65} + \kappa_{62}) - s_{56} s_{65}}$	(10c), (A-7a), (A-8a)
	$\kappa_{oi} = r_i \kappa_{21}$	$\kappa_{21} =$	$\frac{s_{31} \kappa_{23}}{s_{31} + \kappa_{32}}$	$\frac{s_{65} \kappa_{51} \kappa_{26}}{(s_{56} + \kappa_{51})(s_{65} + \kappa_{62}) - s_{56} s_{65}}$	(10d), (A-7b), (A-8b)
Reserve factors	–	$r_i =$	$r_1 + \frac{r_3 s_{13}}{s_{31} + \kappa_{32}}$	$r_1 + \frac{r_5 \kappa_{15}(s_{65} + \kappa_{62}) + r_6 s_{56} \kappa_{15}}{(s_{56} + \kappa_{51})(s_{65} + \kappa_{62}) - s_{56} s_{65}}$	(A-5a), (A-6a)
	–	$r_o =$	$r_2 + \frac{r_3 \kappa_{23}}{s_{31} + \kappa_{32}}$	$r_2 + \frac{r_5 s_{65} \kappa_{26} + r_6 \kappa_{26}(s_{56} + \kappa_{51})}{(s_{56} + \kappa_{51})(s_{65} + \kappa_{62}) - s_{56} s_{65}}$	(A-5b), (A-6b)

The notation for these expressions is defined in Fig. 3, Eqs. (8) and (9), and Fig. 7. Column 1 represents the inverse forms of Eq. (10). To analyze static or "drug"-induced distortion, 3-state expressions should be used when the reaction of interest is immediately adjacent to the charge-carrying reaction, and 4-state expressions should be used if it is separated by unknown reaction steps.

insensitive to experimental manipulation of the rate-limiting reaction. [It need not be stipulated that s_{56} and s_{65} are rate-limiting for the whole transport cycle (so that $s_{56}, s_{65} \ll k^o_{12}, k^o_{21}$), but only for the voltage-independent pathway.] While we cannot specify values for r_i and r_o, some numerical examples, listed in Appendix II, indicate that as long as the lumped reactions in the 4-state model are not strongly asymmetric, then r_i and r_o will be of modest size, lying somewhere between 1 and, say, 10. The second important consequence, which can be seen from Eq. (25a, b), is that any experimental *change* of s_{56} or s_{65}, as induced by a reaction-specific drug, has a proportional effect on the corresponding empirical reaction constant (κ_{io} or κ_{oi}, respectively) from the *I-V* analysis. In order to refer to this kind of result later, we shall call it the *direct* effect. And since the affected empirical constant also points the correct direction around the transport cycle ($\kappa_{io} \propto s_{56}$ and $\kappa_{oi} \propto s_{65}$), we shall also call it *parallel.*

So, for the current-voltage analysis, the overall consequence of experimentally modifying a dominant rate-limiting step (in the voltage-independent pathway) is a direct, parallel effect on the empirical reaction constants. This accords with the intuitive sense that the most effective analysis of a kinetic model in general will be obtained from experiments which manipulate the rate-limiting reaction step.

Consequences of Modifying a Dominant Fast Reaction

This circumstance is much more diverse than that described above; and the results depend strongly on whether the fast step is immediately adjacent to the voltage-dependent reaction or is insulated from it on both sides by slower steps.

In the latter case the overall result is not very much different from that already discussed, and since the labor of algebra in handling the pseudo-4-state model is large relative to the yield of insight, we shall simply summarize the results here. Referring again to Fig. 7*C* and the right-hand column of Table 1, and letting $s_{56}, s_{65} \gg \kappa_{15}, \kappa_{51}, \kappa_{26}, \kappa_{62}$, the 2-state reserve factors (r_i and r_o) are sensitive to both s_{56} and s_{65}, but not very sensitive, since both reaction constants appear simply in both the numerator and the denominator of r_i and r_o. This means that experimental changes of s_{56} or s_{65} have only a weak influence on the voltage-dependent reaction constants (k_{io} and k_{oi}); and that influence is zero if the fast reaction is strongly asymmetric ($s_{56} \gg s_{65}$, or *vice versa*). Therefore, the predominant effect of experimentally modifying s_{56} or s_{65} is again a direct effect, on the lumped reaction constants κ_{io} and κ_{oi}. That effect, however, is not necessarily exactly proportional to the change of s_{56} or s_{65}, and it also need not point in the same direction around the transport cycle. But complications of this sort are more easily treated by the pseudo-3-state model, for the condition that the affected fast reaction is immediately adjacent to the voltage-dependent reaction.

The nomenclature for this treatment is given in Fig. 7*A* and the "3-state" column of Table 1. In the case that $s_{13}, s_{31} \gg \kappa_{23}, \kappa_{32}$, the reserve factor and lumped reaction constants in Table 1 reduce to

$$r_i = r_1 + r_3 \frac{s_{13}}{s_{31}} \quad \text{and} \quad r_o = r_2, \tag{31a, b}$$

and

$$\kappa_{12} = \kappa_{32} \frac{s_{13}}{s_{31}} \quad \text{and} \quad \kappa_{21} = \kappa_{23} \tag{32a, b}$$

in which r_1, r_2 and r_3 are the 3-state reserve factors [*see* Appendix I, Eq. (A3-4b)], which are by definition independent of s_{13} and s_{31}. It will be useful, also, to write out explicitly one more set of results. The empirical voltage-independent reaction constants are

$$\kappa_{io} = \kappa_{32} \cdot r_2 \frac{s_{13}}{s_{31}} \quad \text{and} \quad \kappa_{oi} = \kappa_{23} \left(r_1 + r_3 \frac{s_{13}}{s_{31}} \right). \tag{33a, b}$$

It is evident, from Eqs. (31) and (33), that one case is simpler than all others here: when $s_{31} \gg s_{13}$, which means that the fast reaction step is energetically downhill in a direction pointing *toward* the voltage-dependent step. Then, in addition to r_o, both r_i and κ_{oi} become independent of the fast reaction constants. Once again, the only effect that experimental manipulation of s_{13} or s_{31} can have on the empirical constants is direct, which means upon the voltage-independent constants. However, the circumstance differs from that for a dominant slow reaction, as discussed with Eqs. (29) and (30) above, in that both s_{13} and s_{31} impinge on the single empirical constant κ_{io}. This means that a change of s_{31} must appear as a change of the empirical constant which points in the opposite direction around the transport cycle. Such an effect can be termed *antiparallel.* It should be noted, too, that κ_{io} increases with s_{13}, but decreases as s_{31} increases; so not only the direction but also the sign of the effect can vary. We describe these two cases, respectively, as *positive* and *negative* (*see* Table 2).

The other limiting situation, which brackets the general case of a symmetric fast reaction, is that in which $s_{13} \gg s_{31}$, meaning that the reaction is energetically downhill in a direction pointing *away* from the voltage-dependent step. This has the formal consequence of dropping the 3-state reserve factor r_1

Table 2. Influence of concealed reaction steps[a] upon parameters from a pseudo-2-state kinetic model

	s_{io}, s_{oi} Small (rate-limiting reaction)		s_{io}, s_{oi} Large (fastest reaction)					
			Nonadjacent (4-state)		Adjacent (3-state)			
	Δs_{io}	Δs_{oi}	Δs_{io}	Δs_{oi}	$s_{oi} \gg s_{io}$		$s_{io} \gg s_{oi}$	
					Δs_{io}	Δs_{oi}	Δs_{io}	Δs_{oi}
Direct effect (κ_{io}, κ_{oi})	P+	P+	P+/A−	P+/A−	P+	A−	P+/A+	P−/A−
Transfer effect (k_{oi}, k_{io})	○	○	~○	~○	○	○	P+	A−
Reversal potentials								
E_n	+	−	+	−	+	−	○	○
E_c	○	○	~○	~○	○	○	+	−

[a] The kinetic symbols are defined in Figs. 7 and 8. $s_{io}=s_{13}$ or s_{56} in Fig. 7, and $s_{oi}=s_{31}$ or s_{65} in Fig. 7.
P = Parallel, means the parameter observed to change points in the same direction (around the transport cycle) as the affected s.
A = Antiparallel, means the parameter observed to change points in the opposite direction from the affected s.
+ = positive, means the observed change is an increase of s increases, and a decrease if s decreases.
− = negative, means the observed change is a decrease if s increases, and an increase if s decreases.

out of Eq. (31a) and (33b); and it turns out to be an exceedingly important case for general kinetic modeling.

When $s_{13} \gg s_{31}$, three of the four empirical reaction constants are proportional to the ratio s_{13}/s_{31}, while only one ($k_{io}=r_o k_{12}$) is *in*dependent of both s_{13} and s_{31}. In other words, three of the four empirical constants contain a static distortion, which is proportional to the ratio s_{13}/s_{31}, and upon which effects due to changes of s_{13} or s_{31} must be superimposed. Because s_{13} appears always in the numerator and s_{31} always in the denominator, changes of the former always have a positive effect on the empirical constants, while changes of the latter always have a negative effect. The direct effects (i.e., those upon κ_{io} or κ_{oi}) of changing either s_{13} or s_{31} are both parallel and antiparallel.

The most significant result, however, is that the empirical constant k_{oi}, pointing in the same direction as s_{13}, is also distorted by the ratio s_{13}/s_{31}. Thus, both the static asymmetry of the fast reaction and any experimentally imposed changes of s_{13} or s_{31} are transmitted from the voltage-independent reaction steps to the voltage-dependent reaction by the technique of current-voltage analysis, or, in general, a 2-state analysis. This phenomenon can be called the *transfer* effect. It is parallel-positive for changes of s_{13}, and antiparallel-negative for changes of s_{31}. The fact that k_{io} is not affected by s_{13} and s_{31} means, furthermore, that the energetic transition inherent in the asymmetry of the fast reaction step also appears misplaced to the voltage-dependent reaction. The result can be seen formally by substituting Eqs. (31) and (33) (r_1 dropped out) into Eq. (16a, b) to get the reversal potentials for the change-transit and neutral pathways:

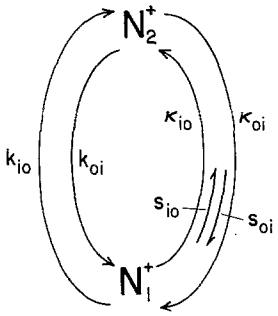

Fig. 8. Augmented 2-state model. Further reduction of the diagram of Fig. 7 to indicate the relationship between the pseudo-3- and 4-state models and the pseudo-2-state model of Fig. 3. Symbolic notation is keyed to Fig. 3 and Table 2

$$E_c = \frac{RT}{zF} \ln \frac{k_{21}}{k_{12}} \left(\frac{r_3}{r_2} \frac{s_{13}}{s_{31}} \right) \quad \text{and} \quad E_n = \frac{RT}{F} \ln \frac{\kappa_{32}}{\kappa_{23}} \left(\frac{r_2}{r_3} \right). \tag{34a, b}$$

This kind of kinetic distortion is capable of accounting for a number of puzzling observations on transport systems, particularly the fact that membrane potential and chemical gradients of ions can appear interchangeable in their effects (*see below*).

The various kinetic relationships defined and developed with Eqs. (29)–(33) are summarized in Table 2 and Fig. 8.

Ion-Motive Forces, and the Kinetic Equivalence of Chemical and Electrical Gradients

As has already been mentioned, cyclic transport processes have traditionally been conceptualized in

terms of two distinct kinds of reaction steps: vectorial steps, which traverse the membrane and therefore, when ions are involved, interact with the transmembrane electric field; and scalar steps, such as ion binding or protein phosphorylation, which can take place in a thin plane parallel to the membrane surface and are not primarily affected by the transmembrane field. In a theoretical sense this distinction may not be absolutely clean (since, e.g., most membrane-bound enzymes or carriers can be expected to be at least weakly dipolar and therefore under stress in the membrane's electric field) [19], but in a practical sense the distinction must be retained. The electric field across the membrane must influence two reaction constants: $k_{12}=k_{12}^o \exp(zu/2)$ and $k_{21}=k_{21}^o \exp(-zu/2)$, whereas any particular chemical concentration will normally influence only one reaction constant: e.g., $[H^+]_o \rightarrow k_{62}$ and $[ATP] \rightarrow k_{53}$, in Figs. 1*A* and 2*A*. It is a remarkable fact, therefore, that many different lines of research have shown a kinetic *equivalence* between the electrical potential difference ($\Delta\psi$) and the chemical potential difference ($RT\ln[X^+]_i/[X^+]_o$) acting to drive one species of ion, *viz.* protons, through a variety of transport systems [17, 29, 42, 54, 58, 72, 81].

Particularly in the literature of bioenergetics, this equivalence has served to legitimize a special terminology, the protonmotive force (ΔP or PMF), which was proposed by Mitchell [62–64] as an alternative to the "electrochemical potential difference for protons," ($\Delta\bar{\mu}_{H^+}$):

$$\text{PMF} \equiv \Delta P \equiv \Delta\bar{\mu}_{H^+}/F = \Delta\psi + \frac{RT}{F}\ln\frac{[H^+]_i}{[H^+]_o}$$
$$= \Delta\psi - 2.303\frac{RT}{F}\Delta\text{pH}. \quad (35)$$

Because of the dominant influence that the notion of PMF has had upon research in active transport and energy coupling over the past ten years, it is of primary importance to examine how the equivalence of chemical and electrical driving forces for ions can emerge from simple kinetic models. (For historical reasons, the discussion that follows will use H^+ as a specific ion; but the arguments apply to any species, adjusted, if necessary, for different valences.)

Another way of stating the observation that $\Delta\psi$ and ΔpH are kinetically equivalent is to say that flux experiments cannot distinguish between them. The discussion of the previous section suggests that the main cause for this may be that the charge-transit reaction is immediately followed by a fast dissociation step. When the paired reassociation is slow, the two-state kinetic analysis will find the energetic transition of the association/dissociation reaction transferred to the charge-transit step, as summarized in the right-hand columns of Table 2. In order for the reasoning to accommodate both intracellular and extracellular concentrations of the transported ion (and therefore, e.g., the transmembrane Δ pH), it is necessary to assume a fast dissociation step on each side, with the two connected (to complete the cycle) by a slow, voltage-independent step. Thus, the minimal kinetic model which will suffice is a pseudo-4-state model, which is diagrammed in Fig. 9.

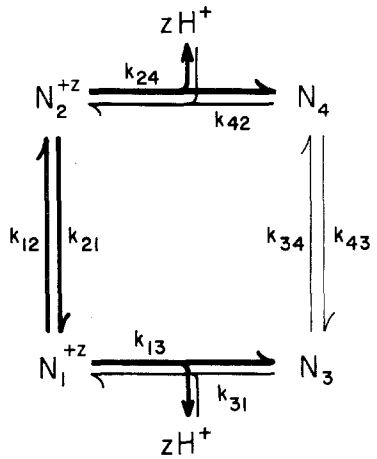

Conditions for kinetic equivalence of $\Delta\psi$, ΔpH

$$k_{12}^o, k_{21}^o \lesssim k_{13}, k_{24}$$
$$k_{13}, k_{24} \gg k_{31}, k_{42}$$
$$k_{31}, k_{42} \lesssim k_{34}, k_{43}$$

$$k_{12}=k_{12}^o \exp\left(\frac{zu}{2}\right),\ k_{21}=k_{21}^o \exp\left(-\frac{zu}{2}\right)$$

$$k_{42}=k'_{42}[H^+]_o^z,\ k_{31}=k'_{31}[H^+]_i^z$$

k_{34}, k_{43} are lumped constants

Fig. 9. Diagram, using generalized pseudo-4-state model, of the arrangement of rate constants which yields kinetic equivalence of membrane potential and the concentration gradient for the transported ion. The carrier decharging steps (k_{13}, k_{24}) must be fast relative to all other voltage-independent steps, and charge transit of the membrane must not be slow

This model is a reduction of the 5- and 6-state models of Figs. 1 and 2, using a generalized nomenclature (*see* end of Appendix I) in which all steps involving ATP or cosubstrate are combined into the transition $N_3 \rightleftharpoons N_4$, so the reaction constants k_{34} and k_{43} are lumped constants. There are two ways in which to proceed with the steady-state analysis of this system: a) via calculation of two-state reserve factors and empirical reaction constants (similar to Table 1, but for the condition of two fast reactions separated by a slow one), or b) by brute-force algebraic analysis of the four-state model itself, using the expanded *I-V* expression of Eq. (A-10) in the Appendix. For present purposes, the latter procedure is simpler.

Formal Derivation

The primary size-ordering of reaction constants that is required to produce equivalence of $\Delta\psi$ and ΔpH

is $k_{13}, k_{24} \gg k_{31}$, k_{42}, k_{34}, k_{43}, but considerable algebraic simplification occurs for a somewhat stronger condition: k_{13}, $k_{24} \gg k_{31}$, $k_{42} \gg k_{34}$, k_{43}. With this assumption, Eq. (A-10) becomes

$$i = zFN \cdot \frac{k_{24}k_{31}k_{43}k_{12} - k_{13}k_{42}k_{34}k_{21}}{r_4 k_{24}k_{31}k_{12} + r_3 k_{13}k_{42}k_{21} + k_{13}k_{24}(k_{34}r_4 + k_{43}r_3)}. \quad (36)$$

In order to include the electric potential and proton concentrations explicitly, we write

$$k_{12} = k^o_{12} \exp(zu/2) \quad \text{and} \quad k_{21} = k^o_{21} \exp(-zu/2), \quad (37\text{a, b})$$

which are analogous with Eq. (11a, b), and

$$k_{31} = k'_{31}[H^+]_i^z \quad \text{and} \quad k_{42} = k'_{42}[H^+]_o^z. \quad (38\text{a, b})$$

After these substitutions, the whole equation can be simplified to the form of Eq. (13) by defining empirical (2-state) reaction constants as follows:

$$k^o_{io} = r_4 k_{24} k'_{31} k^o_{12} \quad \text{and} \quad k^o_{oi} = r_3 k_{13} k'_{42} k^o_{21}, \quad (39\text{a, b})$$

$$\kappa_{io} = Ck_{34}/r_3 \quad \text{and} \quad \kappa_{oi} = Ck_{43}/r_4, \quad (40\text{a, b})$$

with the auxiliary constant

$$C \equiv k_{13}k_{24}r_3 r_4. \quad (41)$$

Finally, Eq. (36) becomes

$$i = \frac{zFN}{C} \cdot \frac{\kappa_{oi}k^o_{io}[H^+]_i^z \exp(zu/2) - \kappa_{io}k^o_{oi}[H^+]_o^z \exp(-zu/2)}{k^o_{io}[H^+]_i^z \exp(zu/2) + k^o_{oi}[H^+]_o^z \exp(-zu/2) + \kappa_{io} + \kappa_{oi}}. \quad (42)$$

Now, just as a "reduced", dimensionless, electromotive force (u) can be defined by Eq. (12), so a "reduced" protonmotive force (p) can be defined as

$$p = F\Delta P/RT. \quad (43)$$

From this definition, and Eq. (35), it follows that

$$\exp\left(\frac{zu}{2}\right) = \left(\frac{[H^+]_o}{[H^+]_i}\right)^{z/2} \exp\left(\frac{zp}{2}\right)$$

and (44a, b)

$$\exp\left(-\frac{zu}{2}\right) = \left(\frac{[H^+]_i}{[H^+]_o}\right)^{z/2} \exp\left(-\frac{zp}{2}\right).$$

Substituting these expressions into Eq. (42), and dividing through by $([H^+]_i \cdot [H^+]_o)^{z/2}$ gives

$$i = \frac{zFN}{C} \cdot \frac{\kappa_{oi}k^o_{io}\exp\left(\frac{zp}{2}\right) - \kappa_{io}k^o_{oi}\exp\left(-\frac{zp}{2}\right)}{k^o_{io}\exp\left(\frac{zp}{2}\right) + k^o_{oi}\exp\left(-\frac{zp}{2}\right) + \frac{\kappa_{io}+\kappa_{oi}}{([H^+]_i \cdot [H^+]_o)^{z/2}}}, \quad (45)$$

which is the final general expression describing the kinetic equivalence of the electrical and chemical gradients for protons. Again, it will be useful to define an auxiliary parameter (R), for the last term in the denominator:

$$R \equiv \frac{\kappa_{io} + \kappa_{oi}}{([H^+]_i \cdot [H^+]_o)^{z/2}}. \quad (46)$$

Practical Conditions

For the special circumstance that $[H^+]_i$ and $[H^+]_o$ can both be changed simultaneously, such that their product is held constant, Eq. (45) shows that $\Delta\psi$ and ΔpH are completely equivalent and interchangeable in their kinetic effects. This is an artificial condition, however, which can rarely be satisfied in experiments, so that a much more satisfactory condition is that the ratio R be kept small with respect to either of the other terms in the denominator. This preserves the equivalence of $\Delta\psi$ and ΔpH when *either* $[H^+]_i$ or $[H^+]_o$ is varied, independently of the other. Referring to Eqs. (39)–(41), the most general circumstance leading to small values of R is that the reaction constants, k^o_{12} and k^o_{21}, for the charge-transfer reaction must be large: at least the order of magnitude of the H^+-dissociation constants, k_{13} and k_{24}. In other words, $\Delta\psi$ and ΔpH become kinetically equivalent when the reaction constants in the pseudo-4-state model are ordered as indicated in Fig. 9. The condition that k^o_{12} and k^o_{21} be large is exactly that discussed previously [*see* Geometric Properties ..., Eqs. (24)–(26)] in which the fundamental current-voltage relationship approaches a hyperbolic tangent function.

In order to illustrate some of the conclusions which can be drawn from Eq. (45), to explore the range of parameter (k^o_{12}, k^o_{21}) values and proton concentrations over which it is valid, and to examine the form of deviations, we have plotted out several sets of current-potential (*I-P*) curves, in Fig. 10. For convenience, the 4-state reaction constants have been selected symmetrically ($k^o_{12} = k^o_{21}$,

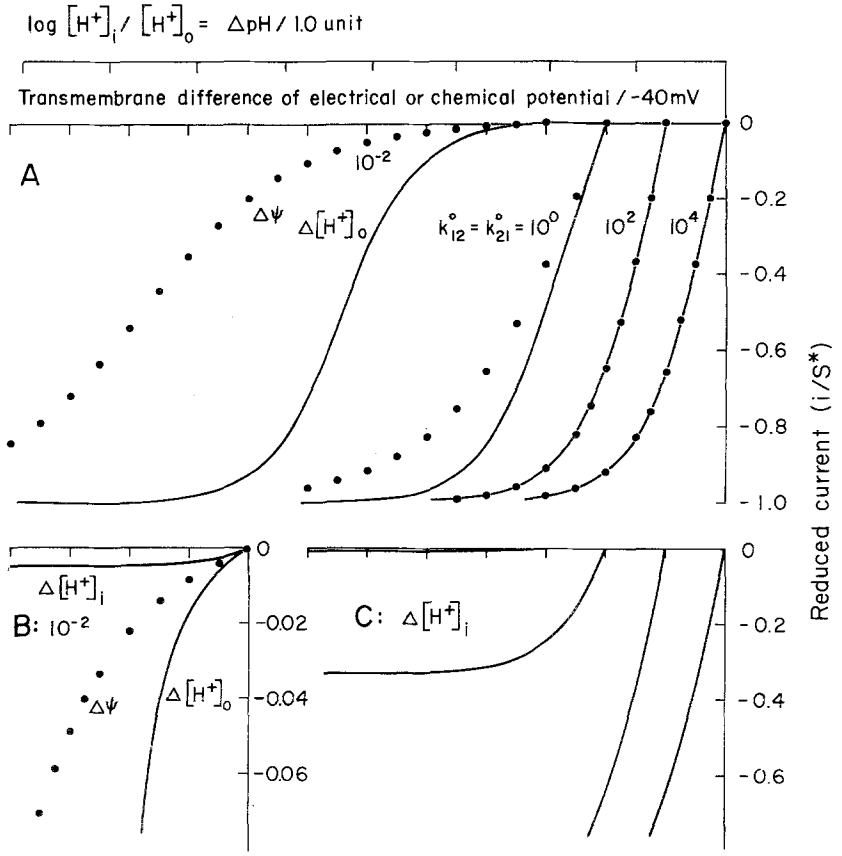

Fig. 10. Demonstration, for a proton-transport system, of the limits on kinetic equivalence of membrane potential ($\Delta\psi$) and the transmembrane pH difference (ΔpH). Curves calculated for a transport system in which the (electrochemical) potential difference for protons acts to drive ATP synthesis or cosubstrate accumulation. The ordinate scale is "reduced" by S^*, as defined in the legend to Fig. 5. All curves plot Eq. (42) [or Eq. (45)], representing the pseudo-2-state form of the 4-state model in Fig. 9. Parameter values used for calculation are listed in Table 3. The reversal potential (E_r) in all cases is 0 mV, and the origin for the different curve-pairs is displaced along the voltage axis solely to give clarity. *Dots:* currents calculated as functions of membrane potential. *Solid Curves:* currents calculated as functions of *extra*cellular (*A*) or *intra*cellular (*C*) proton concentration, and plotted against the transmembrane ΔpH. Each pair is for one value of the zero-voltage reaction constants (k^o_{12}, k^o_{21}), as designated in the Figure. In *B* the three curves for $k^o_{12}=k^o_{21}=10^{-2}$/sec are compared on a 10-fold expanded current scale, showing that there is no significant span in which equivalent currents flow in response to equivalent changes of $\Delta\psi$ and ΔpH. Note that reducing k^o_{12}, k^o_{21} below 10^2 has two pronounced effects: to disequalize the effects of equivalent changes of membrane potential or proton concentration (compare curve pairs in *A*), and to produce an asymmetric response to changes of internal, *versus* external, pH (*compare C* and *A*)

$k_{13}=k_{24}$, $k'_{31}=k'_{42}$, and $k_{34}=k_{43}$), which makes the reversal potential (E_r) equal to zero, for the system. The actual values chosen for the 4-state parameters, and calculated for the corresponding 2-state parameters [Eqs. (39)–(41)], are arrayed in Table 3. For the sake of compactness, calculated curves have been plotted only in the negative quadrant (lower left) on the current-potential axes. This is the region in which $\Delta\bar{\mu}_{H^+}$ is degraded to synthesize ATP or to drive cosubstrate inward through the membrane (*see* Fig. 1), and is the region in which most experimental data for proton-transport systems have been obtained. [The curves, however, project symmetrically into the positive, "ion-pump" quadrant, since κ_{io} and κ_{oi} are equal (*see* discussion of Figs. 4 and 5).]

In Fig. 10*A*, curves calculated with variations of $[H^+]_o$ (acidification) are drawn solid, and curves calculated with variations of $\Delta\psi$ are shown as the plotted points. It is obvious that, when k^o_{12} and k^o_{21} are large (10^2, 10^4; $\geq k_{13}$, k_{24}), the $\Delta\psi$- and $\Delta[H^+]_o$-curves coincide identically; and for most experimental purposes, they probably could be considered equivalent even with k^o_{12}, k^o_{21} of modest size (10^o, so that k^o_{io}, $k^o_{oi} \simeq \kappa_{io}$, κ_{oi}), at least for potential displacements limited to the range of -60 mV. However, as k^o_{12}, k^o_{21} become still smaller (here, 10^{-2}), so that the R term comes to dominate the denominator of Eq. (45), the $\Delta\psi$-curve shows progressively smaller currents (absolute value) than the $\Delta[H^+]_o$-curve. This fact is emphasized by the expan-

Table 3. Parameter values used to generate current-potential curves for comparing kinetic effects of $\Delta\psi$ and ΔpH (Fig. 10)

4-State parameters	Value	2-State parameters	Value
$k^o_{12}=k^o_{21}$	$10^4 \rightarrow 10^{-2}\,\mathrm{sec}^{-1}$	k^o_{io}	$10^{2.5}\cdot k^o_{12}$
$k_{13}=k_{24}$	10^2	k^o_{oi}	$10^{2.5}\cdot k^o_{21}$
$k'_{31}=k'_{42}$	10^7	κ_{io}	$10^{2.5}$
$k_{34}=k_{43}$	10^{-2}	κ_{oi}	$10^{2.5}$
$r_3=r_4$	$10^{0.5}$ [a]	C	10^5
z	1	N	10^{-8} [c]
$[H^+]_i$	10 M [b]		
$[H^+]_o$	10^{-7}		
$\Delta\psi$	0 mV		

[a] Chosen as a reasonable estimate of the reserve factors. The actual size does not matter, since any value can be compensated by suitable 4-state k's. *See Derivation of Pseudo 3-...*, and Appendix II.

[b] These are starting values of $[H^+]_i$, $[H^+]_o$, and $\Delta\psi$. In computations $\Delta\psi$ is varied with both proton concentrations held at 10^{-7}; and each proton concentration is varied with the other held at 10^{-7} and $\Delta\psi$ held at 0.

[c] Because in the plotted curves i is divided by S^* [*see* Eq. (24)], this value has no effect on Fig. 10.

ded diagram of Fig. 10*B*, where even very small displacements of potential give different results for $\Delta\psi$ and $\Delta[H^+]_o$. Another important property of the kinetic model which emerges from Eq. (45) is displayed in Fig. 10*C*. Here, $[H^+]_i$ is lowered (alkalinization) in order to produce the change of chemical potential. It is evident, by comparison with Fig. 10*A*, that as long as k^o_{12}, k^o_{21} are large, the $\Delta[H^+]_i$-curves overlie the $\Delta[H^+]_o$-curves, so that current (or ion flux) can either be "pushed" or "pulled" through the membrane with equal ease. But as k^o_{12}, k^o_{21} fall, the $\Delta[H^+]_i$-curves show even less current (absolute value) than the $\Delta\psi$-curves: the reaction can be "pushed" by $[H^+]_o$, but not easily "pulled" by $\Delta[H^+]_i$, Under this condition, the system could be described as a *chemical rectifier*. It must be emphasized that this chemical rectification does not depend on any input of chemical-bond energy, since the reversal potential for this system is kept at zero.

Associated with the apparent kinetic equivalence of $\Delta\psi$ and ΔpH, in much of the literature of transport and bioenergetics, is a curious proportionality between ΔP (PMF) and either the flux itself (current, ATP synthesis) or the logarithm of the flux. Eq. (45) and Fig. 10 give a straightforward accounting of the linear proportionality. It is exactly to be expected under the condition that the overall *I-P* curve approximates $\tanh(zp/2)$, although the region of practical linearity should be restricted to about 40 mV displacement from E_r, for $z=1$ (less for $z>1$). Log-linearity, however, is *not* so easy to account for by the symmetric model shown in Fig. 9. It can easily be shown that, for small values of k^o_{12}, k^o_{21}, the $\Delta\psi$-curve does display log-linearity away from the reversal potential; when R is much larger than the other terms of the denominator, Eq. (45) becomes

$$i=\frac{zFN}{C}\frac{([H^+]_i\cdot[H^+]_o)^{z/2}}{\kappa_{io}+\kappa_{oi}}\cdot\left(\kappa_{oi}k^o_{io}\exp\left(\frac{zp}{2}\right)-\kappa_{io}k^o_{oi}\exp\left(-\frac{zp}{2}\right)\right). \quad (47)$$

And as p is made negative enough for the first exponential term to be neglected,

$$i=-\frac{zFN}{C}\cdot\frac{([H^+]_i\cdot[H^+]_o)^{z/2}}{\kappa_{io}+\kappa_{oi}}\kappa_{io}k^o_{oi}\exp\left(-\frac{zp}{2}\right). \quad (48)$$

Therefore, the logarithm of the current is proportional to p, but again, strictly so only when the product $[H^+]_i\cdot[H^+]_o$ is held constant. This condition is satisfied for changes of membrane potential, but not for changes in the chemical potential of protons, made in the usual fashion. Thus, Eq. (45) predicts that in general the condition of log-linear dependence between i and ΔP should not exist *simultaneously* with kinetic equivalence of $\Delta\psi$ and ΔpH.

Qualitative Analysis of Published Cases

In practice, however, other factors can enter into the determination of the apparent linear or log-linear relationship between current through an ion transport system and the electrical or chemical driving force. Probably the most important factor is asymmetry which may be superimposed on the general order-of-magnitude relationships among the rate constants indicated in the diagram of Fig. 9 and used for calculation in Fig. 10. In order to demonstrate the influence of reaction asymmetry on the shapes of practical *I-V* curves, we have analyzed four sets of published data.

Two of these are plotted in Fig. 11*A*. Plot *a* is redrawn from Schwab and Komor [81], on the proton-sugar cotransport system in *Chlorella vulgaris*. The open circles represent changes of transmembrane pH, imposed by different extracellular buffer solutions; and the filled circles represent changes of estimated membrane potential, imposed by different solutions of potassium citrate. While it is evident that all the data lie on a common straight line, the most remarkable feature of the plot, in view of Eq. (45) and Fig. 10, is that the region of approximate linearity extends for at least 120 mV, much longer than can be expected even for a charge-transport stoichiometry of 1 H^+ per turn of the cycle. Plot *b* is

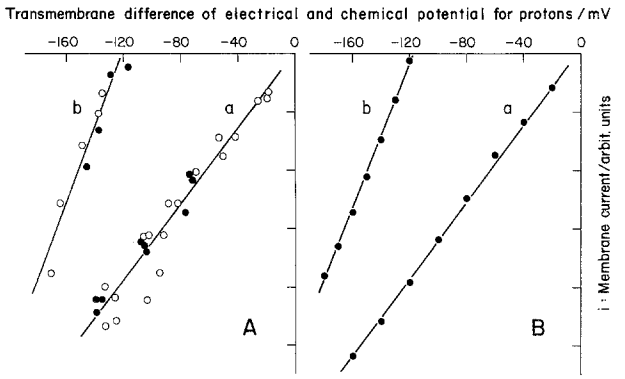

Fig. 11. Two published cases showing kinetic equivalence of $\Delta\psi$ and ΔpH, associated with linear "current-potential" relationships. Open circles (○) represent data obtained by manipulation of extracellular pH; filled circles (●), data obtained by manipulation of membrane potential. Plots made in the lower left quadrant to indicate that the proton gradient is being used to drive another flux. (*See* discussion in the legend to Fig. 5 and the text for Fig. 10.) All lines drawn are fitted by least-squares. *A. Curve a:* data from Schwab and Komor [81], Fig. 2, for proton-coupled uptake of 6-deoxyglucose by *Chlorella vulgaris*. The transport system had been induced by 2–3 hr of incubation with glucose, and the uptake of tritiated sugar was determined from several cell samples taken at 30-sec intervals. Extracellular pH was set at different values between 8.2 and 6 (○), for cells with membrane potentials poised at −74 mV; or membrane potential was varied (●) by preincubation in different concentrations of potassium citrate, with extracellular pH buffered near 7.1. Intracellular pH under closely related conditions was estimated at 7.1 [48]. Five units on the ordinate scale here corresponds to 100% (maximal influx) in the original plots. *Curve b:* data from Lanyi and Silverman [54], Fig. 2, for proton-coupled sodium extrusion by envelope vesicles of *Halobacterium halobium*. In one set of experiments (○), vesicles were loaded with 3 M NaCl and suspended in 2.88 M NaCl/0.12 M KCl at $pH_o = 6.2$, with 5 μM valinomycin. In the other set (●), vesicles were loaded with 1.5 M NaCl/1.5 M KCl and suspended in 2.85 M NaCl/0.15 M KCl at $pH_o = 6.2$. Intracellular pH or membrane potential was then manipulated by incubation at different light intensities (ΔP created by the resident bacterial rhodopsin). Net efflux of sodium was determined by flame analysis of suspension aliquots taken at intervals of several minutes. 5 units on the ordinate scale corresponds to a net efflux of 0.5 μmole/min mg protein in the original plots. *B.* Simulation of the linear relationships in Part *A* by means of Eq. (42) or (13) (only $\Delta\psi$ changed). Ordinate scale reduced by S^*, as in Figs. 5 and 10. Suitable parameters were found in two passes by trial and error as follows:

	k^o_{io}	k^o_{oi}	κ_{oi}	κ_{io}	z
Curve a	1.25	125	1000	10	1
Curve b	1000	10	100	100	1

redrawn from Lanyi and Silverman [54], on the electrogenic $H^+ - Na^+$ countertransport system of *Halobacterium halobium*. Again, the open circles represent changes of ΔpH; and the filled circles, changes of $\Delta\psi$. For these data the span of approximate linearity is short enough (less than 60 mV) to be simply accommodated by a stoichiometry of 1

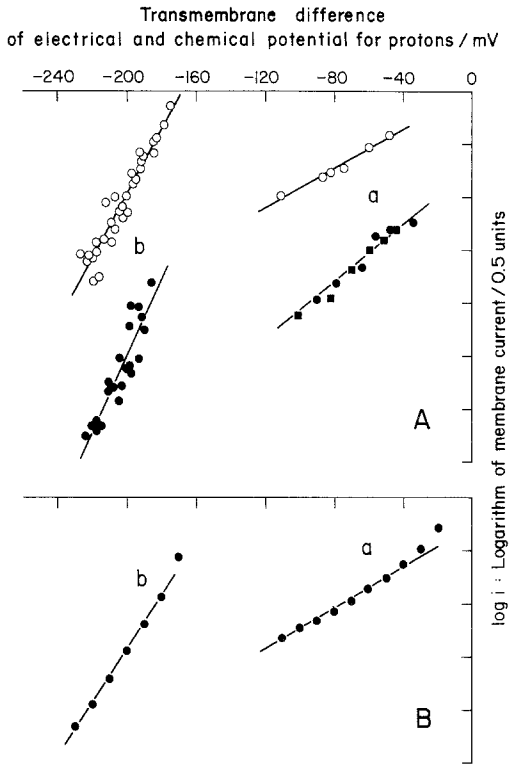

Fig. 12. Two published cases showing kinetic quasi-equivalence of $\Delta\psi$ and ΔpH, associated with log-linear current-potential relationships. Positioning of the plots along the abscissa (potential axis) is the same as that given by the original authors, but separation along the ordinate (logarithm of flux) is made to bring out the differences of slope. (This can be seen best when the plots are sighted end-on.) Symbols as in Fig. 11. *A. Curve a:* data from Robertson et al. [72], Fig. 3 insets, for proton-coupled uptake of lactose by membrane vesicles of *Escherichia coli*. Data in the original plots were maximal velocites for uptake of ^{14}C-lactose determined from full-scale kinetic experiments. Membrane potential was manipulated by adding various concentrations of valinomycin (0.1 to 1 μM) to vesicles suspended in potassium phosphate at pH 5.5 (●) or 7.5 (■), with internal pH fixed at the same value by 0.2 μM nigericin. ΔpH was manipulated (○) at an external pH of 5.5 and a fixed membrane potential of −30 mV, by the converse use of nigericin and valinomycin. The largest fluxes in the original plots were 107, 9, and 10 (nmoles/min mg protein), respectively, for ■, ●, and ○. *Curve b:* data from Maloney and Schattschneider [58], Fig. 2, for proton-driven ATP synthesis by intact cells of *Streptococcus lactis*. Membrane potential was varied (●) by changing extracellular potassium in the presence of valinomycin, and pH_o was controlled (○) by addition of sulfuric acid to the standard phosphate buffer. Maximal ATP synthesis for the two plots as shown was 5.9 and 5.5 (mmoles/min liter cell water), for ○ and ●, respectively. *B.* Rough simulation of the log-linear relationships in Part *A* by means of Eqs. (42) and (13) (only $\Delta\psi$ changed). Steep upward bend of the plots at small currents is an artifact of the ($\log i$)-function, as i goes to zero. Again, the parameters were found in two passes, by trial and error:

	k^o_{io}	k^o_{oi}	κ_{oi}	κ_{io}	z
Curve a	10	1	100	10	1
Curve b	1.1×10^5	9×10^{-5}	30	300	3

charge/cycle (Lanyi and Silverman estimate $2H^+/Na^+$).

Fig. 11*B* displays two theoretical curves (corresponding to the experimental curves just described), calculated from Eq. (42) for variations of $\Delta\psi$, with the proton concentrations held constant. For *b*, curve steepness and the reversal potential of -120 mV led to the following choice of relative magnitudes for the 2-state reaction constants: $k^o_{io}=1000$, $k^o_{oi}=10$, and $\kappa_{io}=\kappa_{oi}=100$. Except for the nonzero reversal potential, this case resembles the curve designated 10^o in Fig. 10*A*. In the case of curve *a* the longer range of linearity demanded an asymmetric *I-V* curve resembling Fig. 5 (curve *A*). The following parameters: $k^o_{io}=1.25$, $k^o_{oi}=125$, $\kappa_{io}=10$, and $\kappa_{oi}=1000$ generate approximate linearity over an adequate range, for both $\Delta\psi$-plots and $\Delta[H^+]_o$-plots, but the predicted slopes for the two differ by a factor of 1.7. We have not attempted to reconcile this discrepancy, because of insufficient knowledge of the detailed data.

Two examples of a log-linear relationship between transport flux and ΔP are shown in Fig. 12*A*. Data for the *a* plots are from Robertson et al. [72], on the H^+-lactose cotransport system in *Escherichia coli*. As in Fig. 11, filled symbols represent $\Delta\psi$-data, and open symbols $\Delta[H^+]_o$-data. The plots have been separated by displacement along the (logarithmic) ordinate scale, in order to reveal the different slopes for electrical and chemical driving forces. Data for the *b* plots are from Maloney and Schattschneider [58], on PMF-driven ATP synthesis in *Streptococcus lactis*. These results emphasize the fact that published data displaying log-linear relationships between transport flux and $\Delta\psi$ or ΔpH also display both a short range (*ca.* 60 mV) for the log-linearity and only an approximate kinetic equivalence for the two driving forces. Such results are at least qualitatively compatible with the discussion of Eq. (48), above. Though we have not attempted to fit Eq. (45) quantitatively to these data, straight lines with roughly the correct slopes (Fig. 12*B*) are generated by the following sets of parameters [Eq. (13)]: Curve *a*, $k^o_{io}=10$, $k^o_{oi}=1$, $\kappa_{io}=10$, $\kappa_{oi}=100$, and $z=1$; Curve *b*, 1.1×10^5, 9×10^{-5}, 300, 30, and 3, in the same order. A surprising outcome of the calculations is that, for the PMF-driven ATP synthesis process in *S. lactis*, a stoichiometry of at least 3 charges/cycle seems required, rather than 2 previously estimated from the same data [58].

Discussion

The schematic model drawn in Fig. 3 may be the simplest plausible kinetic representation for cyclic, carrier-mediated, charge-transport mechanisms in biological membranes. In developing it we have focussed primarily on phenomena directly related to the steady-state charge displacement process: that is, upon current-voltage (*I-V*) characteristics. And we have addressed two major application questions: a) given the fact that all Class I models can be reduced to the pseudo-2-state model (for steady-state *I-V* studies), how can such *I-V* analysis of a pump or cotransport system yield useful information about its underlying kinetic makeup? and b) to what extent can the simple model describe major phenomena reported for pumps and cotransport systems, particularly in the areas of proton transport and bioenergetics? Before finishing discussion of these questions, however, it may be helpful to compare and contrast the formal precedents for the model itself.

Prior Description of Related Processes

The basic strategy for reaction-kinetic modeling of electrogenic carrier-mediated transport processes has been developed by Läuger and his collaborators [56, 87, 88]. In order to apply that strategy to active transport systems, particularly those with unknown kinetic steps, we have made use of the fact that certain classes of reaction intermediates cannot be distinguished in steady-state measurements [11, 89], and have compressed inaccessible reaction constants into "reserve factors." The central relationship [Eq. (13)], which thereby emerges to describe the steady-state current-voltage relationship for Class I models, closely resembles the equation of Läuger and Stark [56] for the steady-state behavior of valinomycin-mediated K^+ transport through lipid bilayer membranes. And, under conditions in which recycling of carriers in electroneutral form is relatively slow [i.e., $\sqrt{k^o_{oi}k^o_{io}}\gg(\kappa_{io}+\kappa_{oi})$], the reaction-kinetic model also resembles ion-exchange models with "mobile" sites [1, 14], as well as less explicit carrier-diffusion models [20].

However, two other familiar reaction-kinetic models for electrogenic primary or secondary active transport give different results. Lieb and Stein [57] have carried out model reduction in a rather restricted form: assuming that only multiple substrate-bound forms of a carrier are indistinguishable by steady-state kinetics. But that, obviously, depends upon the nature of experiments being performed. Given the electrical label for transmembrane charge movement, either multiple unbound forms (Figs. 1 and 3) or multiple bound forms (when the unbound form is charged) can be eliminated for purposes of steady-state *I-V* analysis. Lieb and Stein have for-

mally incorporated the membrane potential into their models, via the expression $k_{io}=k_{oi}\exp(u)$, but have not developed the resultant capability for *I-V* measurement. The expression used is equivalent to our Eq. (11a, b) (for $z=1$) in the case of a "simple carrier" when $k^o_{io}=k^o_{oi}$, but is unlikely to hold for "active" transport systems, where the charge-transfer step can represent a major energetic transition.

The model developed by Heinz and his coworkers [24, 35] – specifically to describe ion-dependent co- (and counter-) transport systems for amino acids – starts with two assumptions: that transmembrane transfer steps are rate-limiting to the overall transport cycle and that ion-binding to the carrier is expressed either mainly as an increased velocity (V_{max}) of cosubstrate transport or mainly as an increased affinity ($1/K_m$) of the carrier for the cosubstrate. The present model [Eqs. (9), (13)], which applies equally to cotransport systems (Fig. 1*B*) and to strictly active transport systems (Fig. 1*A*), is more general in specifically avoiding the assumption that transmembrane transfer steps are rate-limiting. As we shall demonstrate in a subsequent paper (*manuscript in preparation*), it also yields voltage- and ion-dependent changes in the apparent V_{max} and K_m for cosubstrate as a natural consequence of certain choices of reaction constants. The conclusion reached by Heinz, Geck and Wilbrandt [36], that actual cosubstrate accumulation is not possible when the transmembrane transfer steps are not rate-limiting is very surprising to us and appears to arise from the rather stronger assumption that all corresponding carrier forms are in equilibrium across the membrane [36] unless transit steps are rate-limiting. [In Fig. 2*B* above, this would mean $N_2^+ \rightleftharpoons N_1^+$, $N_6=N_5$ and $N_4=N_3$, which raises at least two specific problems: a) it would forbid a steady-state in which the cycle is driven fast in one direction (e.g., by a large transmembrane ionic gradient); and b) it would specifically allow the $N_3 \rightleftharpoons N_4$ transition to short-circuit the $N_2^+ \rightarrow N_1^+$ or $N_5 \rightarrow N_6$ transitions.]

Energy Barriers and Energetic Transitions

Recent attempts to extract structural or kinetic information about intramembranal events from current-voltage plots have focussed largely on localization of the primary energy barrier (=rate-limiting activation energy) to ion diffusion either through channel structures or via solution in the lipid bilayer itself [3, 33, 37, 38]. Reaction-kinetic models for these processes are noncyclic and of the type $S_1^+ \rightleftharpoons S_2^+$, in which there may be several steps between the sites (S) of entry to and exit from the membrane, but all steps lie within the charge-transit pathway itself. In such models overall energetic asymmetry arises only from the electrochemical potential difference for the ion transported, but spatial asymmetry of the activation barrier may be expected (because of structural asymmetry of biological membranes), as well as deviation from a simple Eyring-barrier shape. For example, Hille [37], studying the selectivity of the excitable sodium channels in frog myelinated nerve, was best able to describe the peak *I-V* relationships by a model containing four discrete transitions, in which that representing the largest activation energy is located much closer to the outer face of the membrane than to the inner face. Also, Anderson and Fuchs [3], modeling tetraphenylborate permeation of phospholipid bilayers, concluded that the main barrier to permeation of that lipid-soluble anion is the symmetric "image-force" barrier, but that only a fraction of the total membrane potential is effective.

In a practical sense, however, these conclusions are rarely unique; usually a variety of activation-energy profiles can give rise to *I-V* curves that are (segmentally, at least) indistinguishable [26]. Further constraints can sometimes be obtained, as by examination of nonsteady-state *I-V* data [8], or by generating very precise curves so that higher derivatives (of i with respect to $\Delta\psi$) can be calculated [4]. But even so, technical problems limit the information extractable from *I-V* data.

The same considerations apply, of course, to carrier-mediated transport [79], but additional energy barriers must be taken into account: one for each reaction step in the voltage-independent pathway. And whether one of these, instead of one in the charge-transit pathway, is rate-limiting to the overall cycle determines whether the shape of the current-voltage curve will resemble Fig. 5*D* (κ_{io}, κ_{oi} small) or Fig. 5*E* (κ_{io}, κ_{oi} large). (The energy-barrier terminology is simply an inverse way to describe the relative magnitudes of various pairs of reaction constants.) It is, however, the barrier(s) in the charge-transit pathway which determines the inherent *symmetry* of the overall *I-V* relationship. Symmetric behavior of Eq. (13), as developed in Eq. (23) and (25) and displayed in Fig. 4, depends directly upon symmetry of the exponential terms: that is, upon the choice of 0.5 as the multiplier of zu and $-zu$, rather than the more general fractions δ and $1-\delta$ ($\delta \lesseqgtr 1$). When *I-V* data for a particular system cannot be resolved into symmetric components, the possibility of an asymmetric barrier in the charge-transit pathway should be considered, although *actual* symmetry may become apparent only when a wide span of voltages is explored (say, 150 mV on each side of E_c). A much wider range of *I-V* curve shapes, than those

displayed in Figs. 4 and 5, becomes possible if an asymmetric Eyring barrier is assumed along the charge-transit pathway [32].

From the pseudo-2-state model, a carefully determined steady-state *I-V* curve should yield all four empirical reaction constants, either analytically [via Eqs. (14), (15) and (17)] when a sufficient voltage span is covered, or by statistical optimization (*see* Usefulness and Meaning ...). Application of the latter technique to data for the electrogenic proton pump in *Neurospora* and the electrogenic chloride pump in *Acetabularia* [32] has revealed that $k_{io}^o \gg k_{oi}^o$, whereas $\kappa_{oi} \simeq \kappa_{io}$. In both cases, therefore, the major energetic transition, at which intramolecular energy (of phosphate anydride bonds, for example, or molecular conformation) appears to be converted into gradient energy, occurs during actual charge transit. Assuming that reserve factors do not distort the picture too severely (*see below*), it is interesting to speculate that this arrangement may be general for ion pumps operating against an electrical gradient. Such pumps differ conceptually in an important way from electroneutral pumps or those operating in the absence of an electric field. Pumping ions against a field requires work to be expended on each charge moved, whereas pumping against a concentration gradient expends work only on the ensemble.

As has already been discussed, reliable localization of the major energetic transitions from steady-state *I-V* data requires the reserve factors r_i and r_o to be well-behaved. It is, however, a quantitative matter, not a qualitative one. The influence of reserve factors upon the apparent magnitude of energy input to the charge-transit step can be seen by substituting Eqs. (10a, b) into Eq. (16a):

$$E_c = \frac{RT}{zF} \ln \frac{r_i k_{21}^o}{r_o k_{12}^o}. \tag{49}$$

Numerical evaluation of r_i and r_o, as given in Appendix II, shows that the ratio r_i/r_o stays near unity (i.e., between about 0.3 and 3) except when rapid decharging of the carrier immediately follows transit. And the energy represented by this possible 10-fold error in the ratio $r_i k_{21}^o / r_o k_{12}^o$ is about 60 mV, which is hardly significant compared with E_r values of several hundred millivolts [32].

Applications and General Implications of the Model

Despite its conceptual simplicity, the pseudo-2-state reaction kinetic model for ion pumps and cotransport systems is capable of describing a very wide range of phenomena observed in transport-kinetic experiments. Apart from predicting several types of voltage dependence for the standard enzyme-kinetic parameters of ion-transport systems (*manuscript in preparation*), it can accommodate many different shapes of current-voltage curves over the usual measureable voltage span (*ca.* -200 to $+100$ mV); it can account for kinetic equivalence, or quasi-equivalence, of membrane potential and ion-concentration gradients; it suggests specific extensions, of conventional kinetic data, which can serve as tests for various forms of the model; and it provides a rationale upon which to select various "ideal" models to describe particular systems efficiently.

Referring to the illustrative *I-V* curves in Fig. 5, and focussing on the voltage span just to the right of the reversal potential (E_r), it is obvious that experimental *I-V* relationships can appear linear, hyperbolic, flat, parabolic, or exponential, depending on the length of *I-V* curve sampled, the proximity to E_r, and the relative magnitudes of k_{io}^o, k_{oi}^o *versus* κ_{oi}, κ_{io}. It seems clear, for example, why in most animal cells *I-V* curves for electrogenic sodium pumping resemble "current sources" [52, 61, 92]; they are flat, or parallel to the voltage axis, because the accessible voltage span is far from the reversal potential, and voltage-independent reaction steps are rate-limiting. As long as such a condition prevails across the pumping membrane, any battery-and-resistor representation of the pump (whether couched in thermodynamic or electrical nomenclature) must be a poor approximation. The convenient assumption of a current-source behavior, which is incorporated into many discussions of electrogenic pumps in excitable tissue [2, 12, 22, 65], may therefore be generally justified. On the other hand, the battery-and-resistor may be a good approximation for electrogenic pumps in giant algae [15, 31, 85, 86] where larger accessible membrane potentials (out to -300 mV) and higher stoichiometries ($z>1$) combine to place the usual $I-V$ span close to E_r, under conditions in which recycling of neutral carrier is relatively slow ($\sqrt{k_{io}^o \cdot k_{oi}^o} \gg (\kappa_{oi} + \kappa_{io})$).

Perhaps the most important area into which the model reaches is the description of various proton transport systems, most intensively studied in energy-coupling membranes. We have already explored the central results in this area, in the section Ion-Motive Forces ..., but a few additional points should be made. By means of the pseudo-4-state model, it can be shown that both the kinetic equivalence of $\Delta\psi$ and ΔpH and the linear dependence of i on $\Delta\psi$ or ΔP, for spans of ± 40 mV, are direct kinetic consequences of making the carrier decharging[2] reactions fast [Eqs. (36)–(45)], under conditions

[2] Decharging here means conversion of the carrier from a charged state to an uncharged state. In the case when charge-transit is brought about by the uncomplexed carrier (*see*, e.g., Ref. [32]), decharging consists of ion-association with the carrier, rather than dissociation, as generally depicted in this paper.

when the zero-voltage reaction constants, k^o_{12} and k^o_{21} are not small. (Other special conditions exist for linearity and quasi-equivalence of $\Delta\psi$ and ΔpH: e.g., for variations around E_r, when all reaction constants in the pseudo-4-state model are approximately equal. Thus far, however, we have not discovered any other applicable general conditions.) Linearity over the spans in excess of ± 40 mV, as frequently observed, is more difficult to account for. As shown in Fig. 11 (curves *a*) a span of 120 mV can be handled by choosing the voltage-independent reaction constants in a sufficiently asymmetric fashion. But even longer spans of linearity (*ca.* 200 mV) have been reported, as by Dixon and Al-Awqati [17] for the reversible ATP-driven proton pump in turtle bladder and by Gräber et al. [30] for the coupling ATPase in chloroplasts. In order for the model of Fig. 9 to describe such results, it appears necessary to introduce an asymmetric Eyring barrier (*see* above section) into the charge-transit step: for example, by letting $k_{12}=k^o_{12}\exp(0.9\,zu)$ and $k_{21}=k^o_{21}\exp(-0.1\,zu)$. Whether such an adaptation is actually warranted is unclear, since in both cases the apparent *I-V* relationships may be distorted by tissue geometric factors (serial membranes for the bladder preparation, vesicle-size spread for the chloroplast suspensions).

The wide range of applicability of Eqs. (13) and (45) makes postulation of such special devices as *P*-gates and ion wells [63] unnecessary, at least as explanations of kinetic data. The concept of the proton well, originally devised to produce elevated substrate concentrations for F_1-type ATP synthetases, does yield kinetic equivalence of $\Delta\psi$ and ΔpH, but is circumvented in that role by Eq. (45). Gates associated with pumps or cotransport systems have been postulated many times [e.g., 29, 39, 54], either to account for steep *I-V* relationships, or to account for the practical irreversibility of some pumps. But, as was pointed out in developing Eq. (27), steepness of an *I-V* relationship can be judged only when the saturation current (maximal transport velocity) is known. Lanyi and Silverman [54] have suggested that one kind of gating mechanism could be a stoichiometry of 2 or more charges/cycle ($z>2$). Considering their data already discussed in Fig. 11*A*, however, and assuming 850 nmoles/min mg protein [53] to be the saturating velocity for the H^+-Na^+ countertransport system in *Halobacterium* vesicles, $z=1$ gives a quite satisfactory description (Fig. 11*B*). Finally, gating to account for irreversibility of certain transport systems [29, 30] may simply be a question of kinetic competence. Again referring to Fig. 5, when the empirical voltage-independent reaction constants are asymmetric, i.e., $\kappa_{io}\neq\kappa_{oi}$, transport systems will act either only as pumps (Fig. 5, curve *C*) or only as ion-driven ATP-synthetases or substrate accumulators. When E_r is passed in the unfavorable direction, little current flows despite the theoretical reversibility. It has already been pointed out that such kinetic asymmetry can account for an unexpectedly long span of linearity between i and $\Delta\psi$ or ΔP. It would seem a very important test of this generalized kinetic model to determine whether those systems displaying long spans of linearity coincide with those which appear to be "gated" against reversal.

This work was supported by Research Grant GM-15858 from the National Institute of General Medical Sciences and Research Grant PCM 7913412 from the National Science Foundation, along with travel and stipends to D.G. (Grant G409/7) and U.-P.H. (Grant Ha712/6) from the Deutsche Forschungsgemeinschaft. D.S. was a James Hudson Brown Fellow at the Yale School of Medicine. We are indebted to Dr. H.R. Kaback for access to data cited in Ref. [72] prior to its publication.

Appendix I

Derivation of Pseudo-3- and Pseudo-4-State Models: Relation to the Pseudo-2-State Model

Nomenclature. In order to avoid incrustations with another layer of nomenclature, we shall not present these derivations in the most general form, but instead shall adhere to the nomenclature used in Fig. 7 (as extrapolated from Fig. 2) for the 3-state and 4-state models, and in Eq. (8) for the 2-state model. (The results can easily be translated, by conversion of subscripts, for the 5-state "real" model of the proton pump in Figs. 1*A* and 2*A*, for any of the three equivalent 4-state models associated with Fig. 2*B*, or for any other presumed n-state model.) k_{12} and k_{21} will be used throughout to designate the voltage-dependent rate constants [derived with explicit inclusion of the reserve factors, as discussed for Eqs. (6)–(8)]. s (with numerical subscripts) will designate reaction constants for the additional step that is to be excluded from the lumping procedure; and κ (with numerical subscripts) will denote lumped reaction constants for all other steps. r_1, r_2, ... will be used for the reserve factors in the higher-state models, but to avoid ambiguity r_i and r_o will be retained for the 2-state model.

Finally, for the sake of compactness, the ensemble of steady-state mass equations for 2-, 3-, and 4-state models will be set up —and manipulated, to a certain extent—in matrix notation. Fig. 7*B* will not be dealt with specifically here, since its results can be obtained directly from those for Fig. 7*A* by symmetric substitution.

Steady-State Mass Equations. In the case of the 2-state model, Eqs. (4b), (6), and the complementary equation $-d\mathrm{N}_2^+/\mathrm{dt}=0=-(k_{12}+\kappa_{12})\mathrm{N}_1^+ +(k_{21}+\kappa_{21})\mathrm{N}_2^+$ could have been written as

$$\mathbf{MV}=\mathbf{N}, \tag{A-1}$$

in which the matrix (**M**), and the vectors (**V** and **N**) are defined by

$$\begin{bmatrix} r_i & r_o \\ (k_{12}+\kappa_{12}) & -(k_{21}+\kappa_{21}) \\ -(k_{12}+\kappa_{12}) & (k_{21}+\kappa_{21}) \end{bmatrix} \begin{bmatrix} \mathrm{N}_1^+ \\ \mathrm{N}_2^+ \end{bmatrix} = \begin{bmatrix} N \\ 0 \\ 0 \end{bmatrix}. \tag{A2-0}$$

(A2-1)

(A2-2)

The system could then have been solved for N_1^+ and N_2^+, in Eqs. (7a, b), via the reduced matrix $\mathbf{M}_2$ and vector N_2 obtained by deleting the last row, Eq. (A2-2), above. [The latter equation must be retained in the general case, in order to provide correspondences between the reserve factors in the 2-state and higher-state models (*see below*)]. The solutions can be written as

$$N_j^+ = |^j\mathbf{M}_2|/|\mathbf{M}_2|, \tag{A-2}$$

in which $|\mathbf{M}_2|$ is the determinant of $\mathbf{M}_2$, and $|^j\mathbf{M}_2|$ is the determinant of the matrix obtained by substituting the vector $\mathbf{N}_2$ for the column headed r_j (here $i=1, o=2$) in $\mathbf{M}_2$.

In the case of the 3-state model (counterclockwise, Fig. 7*A*), Eq. (A-1) is written:

$$\begin{bmatrix} r_1 & r_2 & r_3 \\ (k_{12}+s_{13}) & -k_{21} & -s_{31} \\ -k_{12} & (k_{21}+\kappa_{23}) & -\kappa_{32} \\ -s_{13} & -\kappa_{23} & (s_{31}+\kappa_{32}) \end{bmatrix} \begin{bmatrix} N_1^+ \\ N_2^+ \\ N_3 \end{bmatrix} = \begin{bmatrix} N \\ 0 \\ 0 \\ 0 \end{bmatrix}. \tag{A3-0}$$

(A3-1)

(A3-2)

(A3-3)

The determinant solutions for N_1^+, N_2^+, and N_3 are just

$$N_j^{(+)} = |^j\mathbf{M}_3|/|\mathbf{M}_3|. \tag{A-3}$$

And for the 4-state model,

$$\begin{bmatrix} r_1 & r_2 & r_5 & r_6 \\ (k_{12}+\kappa_{15}) & -k_{21} & -\kappa_{51} & 0 \\ -k_{12} & (k_{21}+\kappa_{26}) & 0 & -\kappa_{62} \\ -\kappa_{15} & 0 & (s_{56}+\kappa_{51}) & -s_{65} \\ 0 & -\kappa_{26} & -s_{56} & (s_{65}+\kappa_{62}) \end{bmatrix} \begin{bmatrix} N_1^+ \\ N_2^+ \\ N_5 \\ N_6 \end{bmatrix} = \begin{bmatrix} N \\ 0 \\ 0 \\ 0 \end{bmatrix},$$

and Eqs. (A4-0) through (A4-4)

$$N_j^{(+)} = |^j\mathbf{M}_4|/|\mathbf{M}_4|. \tag{A-4}$$

Interpretation of the Reserve Factors. The same argument is used to generate the reserve factors in the pseudo-3- and 4-state models as in the pseudo-2-state model, but the end points of the summations are different. For the 3-state model, Eq. (4a, b) becomes

$$N = N_1^+ + \sum_{j=1}^{n} r_{j2} N_2^+ + \sum_{j=1}^{n} r_{j3} N_3$$

or (A3-4a, b)

$$N = r_1 N_1^+ + r_2 N_2^+ + r_3 N_3,$$

which incorporates the identities $r_1=1$, $r_{jj}=1$, and $r_{ji}=0$ $(j \neq i)$. For the 4-state model, there are two separate sets of concealed reactions, one bounded by N_2^+ and N_6, and one bounded by N_1^+ and N_5. In this case Eq. (4a, b) becomes

$$N = \sum_{j=2,4\ldots}^{2n} r_{j2} N_2^+ + \sum_{j=2,4\ldots}^{2n} r_{j6} N_6 + \sum_{j=1,3\ldots}^{2n-1} r_{j1} N_1^+ + \sum_{j=1,3\ldots}^{2n-1} r_{j5} N_5 \tag{A4-5a}$$

or

$$N = r_1 N_1^+ + r_2 N_2^+ + r_5 N_5 + r_6 N_6, \tag{A4-5b}$$

again with $r_{jj}=1$ and $r_{ji}=0$ $(j \neq i)$.

The reserve factors in the 2-state model can be expanded from the 3- and 4-state models by the following general procedure. First, using Eq. (A3-3) or Eqs. (A4-3) and (A4-4), solve for N_3 or N_5 and N_6 in terms of N_1^+ and N_2^+. Second, substitute those solutions into Eqs. (A3-4b) or (A4-5b), respectively; and third, make a term-by-term comparison with Eq. (4b). The results of these manipulations are

$$r_i = r_1 + \frac{r_3 s_{13}}{s_{31}+\kappa_{32}} \quad \text{and} \quad r_o = r_2 + \frac{r_3 \kappa_{23}}{s_{31}+\kappa_{32}} \tag{A-5a, b}$$

for the 3-state model; and

$$r_i = r_1 + \frac{r_5 \kappa_{15}(s_{65}+\kappa_{62}) + r_6 s_{56} \kappa_{15}}{(s_{56}+\kappa_{51})(s_{65}+\kappa_{62}) - s_{56} s_{65}} \tag{A-6a}$$

and

$$r_o = r_2 + \frac{r_5 s_{65} \kappa_{26} + r_6 \kappa_{26}(s_{56}+\kappa_{51})}{(s_{56}+\kappa_{51})(s_{65}+\kappa_{62}) - s_{56} s_{65}} \tag{A-6b}$$

for the 4-state model.

Evaluation of Lumped Reaction Constants in the Pseudo-2-State Model. κ_{12} and κ_{21} can be evaluated in much the same fashion as r_i and r_0, though the algebra is somewhat more laborious. First, substitute the 3-state [Eqs. (A-5a, b)] or 4-state [Eqs. (A-6a, b)] values of r_i and r_o into Eq. (7a, b), and multiply the denominators of r_i and r_o into the numerators of N_1^+ and N_2^+, in order to obtain each equation as a simple fraction. Second, calculate N_1^+ and N_2^+ from the 3- or 4-state models, via Eqs. (A-3) or (A-4). Term-by-term comparison of the corresponding numerators then gives the 3- or 4-state equivalences for κ_{12} and κ_{21}. The correctness of the results can be verified with a term-by-term comparison of denominators. From the 3-state model,

$$\kappa_{12} = \frac{s_{13}\kappa_{32}}{s_{31}+\kappa_{32}} \quad \text{and} \quad \kappa_{21} = \frac{s_{31}\kappa_{23}}{s_{31}+\kappa_{32}}. \tag{A-7a, b}$$

From the 4-state model,

$$\kappa_{12} = \frac{s_{56}\kappa_{15}\kappa_{62}}{(s_{56}+\kappa_{51})(s_{65}+\kappa_{62}) - s_{56}s_{65}}$$

and (A-8a, b)

$$\kappa_{21} = \frac{s_{65}\kappa_{51}\kappa_{26}}{(s_{56}+\kappa_{51})(s_{65}+\kappa_{62}) - s_{56}s_{65}}.$$

Generalization of the Model. In the previous paragraphs k, s, and κ have been used as mnemonic nomenclature for reaction constants with different functions in the kinetic model: voltage-dependence, sensitivity to experimental change, and lumping of concealed reactions, respectively. Explicit use is made of this mnemonic device in the text section on interpretation of reserve factors. Also, in order to develop the formal relationships out of conventional kinetic diagrams for pumps and cotransport systems, we have retained the subscripting nomenclature from the 6-state model. For a number of purposes, however, it is more convenient and efficient to use a common designation, say k as shown in Fig. 2, for all reaction constants, and a strictly serial ordering of subscripts. An important case in point, and one which can be used for analysis of data in the literature, is the algebraic expansion of the expression for current flow through any pseudo m-state model. The general result, analogous to Eq. (8), but without $r_i r_o$ multiplied through numerator and denominator, is

$$i = zF \frac{k_{12}|^1\mathbf{M}_m| - k_{21}|^2\mathbf{M}_m|}{|\mathbf{M}_m|}, \tag{A-9}$$

where $m=2, 3, \ldots, n$, for the pseudo m-state models. Unhappily, this compact notation doesn't convey much of an intuitive feeling about the behavior of the underlying kinetic systems; but then neither does the detailed algebraic expansion, whose de-

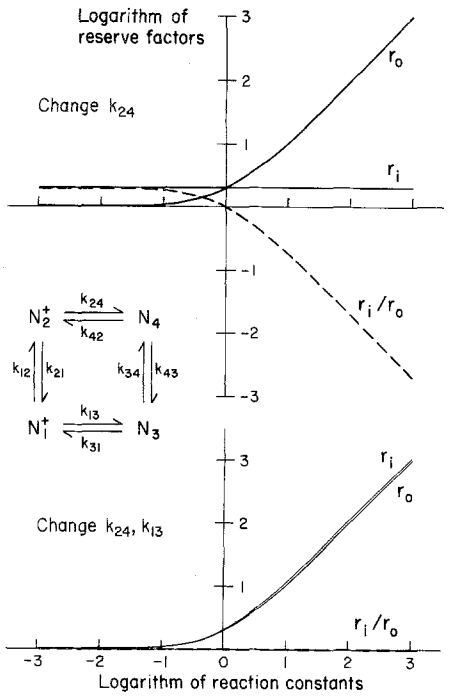

Fig. 13. Numerical evaluation of reserve factors: rapid decharging of the carrier. Two-state reserve factors (r_i, r_o) calculated by means of Eq. (A-6) (*see* Appendix II, or Table 1), using the generalized "real" 4-state kinetic model diagrammed in the *inset*. The reference condition was taken with all 4-state reserve factors omitted, and all voltage-independent reaction constants equal to 1. k_{24} (top), or k_{24} and k_{13} simultaneously (bottom), were then varied from 10^{-3} to 10^3. The ordinate scale is logarithmic simply to accommodate the largest r-values

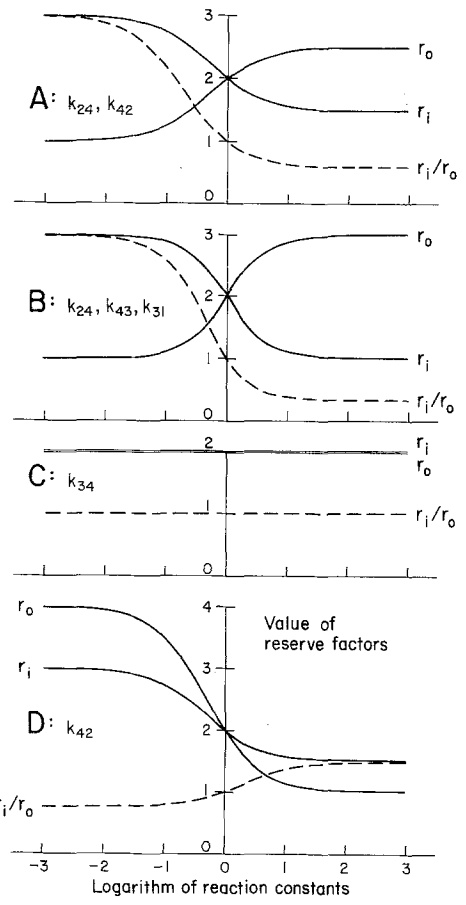

Fig. 14. Numerical evaluation of reserve factors: demonstration of some conditions which give bounded reserve factors. Computations exactly as in Fig. 13, but different constants varied. *A*. Showing that increasing k_{42} simultaneously with k_{24} cancels the major effect of k_{24} on r_o (*compare* Fig. 13). *B*. Showing similar cancellation by simultaneous increase of k_{43} and k_{31} along with k_{24}. *C*. Showing r_i and r_o to be independent of reaction steps not contiguous with the voltage-dependent steps. Complete independence here is a consequence of the symmetry of the 4-state model. *D*. Showing that changing k_{42} alone does not make r_i or r_o large

nominator (for example) contains m^2 terms (which are laid out in numerous books on kinetic models [82]). However, a simple verbal description is possible: 1) The numerator of the fraction in Eq. (A-9) consists of $N\times$ (product of all clockwise reaction constants, minus the product of all counterclockwise reaction constants). 2) The denominator is the sum of m^2 terms, m of them multiplied by each reserve factor, r_x; the m terms corresponding to each reserve factor consist of the products of all combinations of reaction constants, taken $m-1$ at a time, which point *toward* N_x (the carrier state associated with the reserve factor r_x).

Thus, for the generalized 4-state model,

$$i = zFN \frac{k_{24}k_{43}k_{31}k_{12} - k_{13}k_{34}k_{42}k_{21}}{\begin{aligned} &r_1(k_{21}k_{42}(k_{34}+k_{31}) + k_{31}k_{43}(k_{24}+k_{21})) \\ &+r_2(k_{12}k_{31}(k_{43}+k_{42}) + k_{42}k_{34}(k_{13}+k_{12})) \\ &+r_3(k_{13}k_{21}(k_{42}+k_{43}) + k_{43}k_{24}(k_{12}+k_{13})) \\ &+r_4(k_{24}k_{12}(k_{31}+k_{34}) + k_{34}k_{13}(k_{21}+k_{24})) \end{aligned}}. \quad \text{(A-10)}$$

As noted above $r_x \equiv 1$ for any carrier state not involved in a lumping procedure. A somewhat more elaborate diagrammatic statement of these verbal rules has been given by King and Altman [46].

Appendix II

A discussion of how the pseudo-2-state reserve factors behave under certain limiting conditions, with emphasis on their *dynamic* effect upon the apparent magnitudes of the voltage-sensitive reaction constants during experimental manipulation, is given in the text section Usefulness and Meaning.... The purpose of this Appendix is to provide some practical and general rules for the behavior of the reserve factors (when the limiting cases do not apply), with a particular emphasis on their *static* magnitude, as influenced by particular choices of reaction constants in the set of lumped reactions.

The rules outlined below come either directly from the definitions of reserve factors given in Eqs. (4), (5), (A3-4), and (A4-5), or from a survey of values computed for 3-, 4-, and 5-state models via Eqs. (A-5), (A-6), and their 5-state equivalents. The reference condition, or starting point for the computations, was chosen with all 3-, 4-, or 5-state reserve factors equal to 1 (this makes the models "real"), and with all voltage-independent reaction constants also equal to 1. Selected reaction constants were then varied between 0.001 and 1000. Some representative results are plotted in Figs. 13 and 14, for the 4-state model; there were no qualitative differences from the 3- and 5-state models. The no-

tation for reaction constants in a "real" 4-state model is taken from the section on *Generalization...* in Appendix I, and given explicitly in the inset diagram of Fig. 13.

Rules

1) By definition, r_i, $r_o \geqq 1$, always.
2) Also by definition, r_i and r_o are independent of k_{12} and k_{21}.
3) If all reaction constants contained in the lump are equal, then $r_i = r_o = n/2$, where n is the total number of carrier states.
4) r_i and r_o stay small and *bounded* for almost any choice of reaction constants in the lump, *except* when k_{24} or k_{13} becomes large. In other words, the gross magnitude of the reserve factors is controlled by the relative speed of the carrier decharging[2] reaction immediately following charge transit. *This is the most important rule.* The general part is illustrated in Fig. 14, and the exception is illustrated in Fig. 13 (some consequences are listed in Table 2).
5) Starting with all reaction constants = 1, and changing any one constant (except k_{24} or k_{13}), as well as many combinations, between 0 and $+\infty$ leaves r_i and $r_o \leqq 2$ for a 3-state model, $\leqq 4$ for a 4-state model, and $\leqq 7$ for a 5-state model. At the same time, the ratio r_i/r_o stays between 3 and 0.3 (*see* Fig. 14.)
6) k_{24} does not affect r_i, and k_{13} does not affect r_o; but r_i becomes large with k_{13} and r_o becomes large with k_{24} (Fig. 13, top). This means that the ratio r_i/r_o gets very small as k_{24} increases (Fig. 13, top) and gets very large as k_{13} increases.
7) It follows from rule 6 that the ratio r_i/r_o stays bounded if both k_{24} and k_{13} become similarly large. This rule is illustrated for $k_{24} = k_{13}$ in Fig. 13 (bottom).
8) r_o stays bounded despite a large value of k_{24} under two conditions: either the paired reaction constant (k_{42}) is similar to k_{24}, or all other voltage-independent reaction constants pointing in the same direction as k_{24} are similarly large. This rule is illustrated in Fig. 14*A* for $k_{24} = k_{42}$, and in Fig. 14*B* for $k_{24} = k_{43} = k_{31}$. Similar statements apply for r_i and k_{13}.

References

1. Adrian, R.H. 1969. Rectification in muscle membrane. *Prog. Biophys. Mol. Biol.* **19**:339–369
2. Adrian, R.H., Slayman, C.L. 1966. Membrane potential and conductance during transport of sodium, potassium, and rubidium in frog muscle. *J. Physiol. (London)* **184**:970–1014
3. Andersen, O.S., Fuchs, M. 1975. Potential energy barriers to ion transport within lipid bilayers: Studies with tetraphenylborate. *Biophys. J.* **15**:795–830
4. Attwell, D. 1979. Problems in the interpretation of membrane current-voltage relations. *In:* Membrane Transport Processes. C.F. Stevens and R.W. Tsien, editors. Vol. 3, pp. 29–41. Raven Press, New York
5. Baird, B.A., Hammes, G.G. 1979. Structure of oxidative- and photo-phosphorylation coupling factor complexes. *Biochim. Biophys. Acta* **549**:31–53
6. Beck, J.C., Rosen, B.P. 1979. Cation/proton antiport systems in *Escherichia coli:* Properties of the sodium/proton antiports. *Arch. Biochem. Biophys.* **194**:208–214
7. Bentrup, F.W. 1980. Electrogenic membrane transport in plants. A review. *Biophys. Struct. Mechanism* **6**:175–189
8. Benz, R., Läuger, P., Janko, K. 1976. Transport kinetics of hydrophobic ions in lipid bilayer membranes: Charge-pulse relaxation studies. *Biochim. Biophys. Acta* **455**:701–720
9. Boyer, P.D., Stokes, B.O., Wolcott, R.G., Degani, C. 1975. Coupling of "high-energy" phosphate bonds to energy transductions. *Proc. Natl. Acad. Sci. USA* **34**:1711–1717
10. Brey, R.N., Rosen, B.P., Sorenson, E.N. 1980. Cation/proton antiport systems in *Escherichia coli:* Properties of the potassium/proton antiports. *J. Biol. Chem.* **255**:39–44
11. Britton, H.G. 1966. The concept and use of flux measurements in enzyme studies: A theoretical analysis. *Arch. Biochem. Biophys.* **117**:167–183
12. Caldwell, P.C. 1973. Possible mechanisms for the linkage of membrane potentials to metabolism by electrogenic transport processes with special reference to *Ascaris* muscle. *Bioenergetics* **4**:201–209
13. Chapman, J.B., Kootsey, J.M., Johnson, E.A. 1979. A kinetic model for determining the consequences of electrogenic active transport in cardiac muscle. *J. Theor. Biol.* **80**:405–424
14. Conti, F., Eisenman, G. 1966. The steady-state properties of an ion exchange membrane with mobile sites. *Biophys. J.* **6**:227–246
15. Dainty, J., Lannoye, R.J., Tarr, S.E. 1970. Voltage-current characteristics of *Chara australis* during changes of pH and exchange of Ca-Mg in external medium. *J. Exp. Bot.* **21**:558–565
16. Diamond, J.M. 1964. Transport of salt and water in rabbit and guinea pig gall bladder. *J. Gen. Physiol.* **48**:1–14
17. Dixon, T.E., Al-Awqati, Q. 1979. Urinary acidification in turtle bladder is due to a reversible proton-translocating ATPase. *Proc. Natl. Acad. Sci. USA* **76**:3135–3138
18. Eddy, A.A. 1978. Proton-dependent solute transport in microorganisms. *Curr. Top. Membr. Transp.* **10**:279–360
19. Feldberg, S.W., Nakadomari, H. 1977. Charge-pulse studies of transport phenomena in bilayer membranes. II. Detailed theory of steady-state behavior and application to valinomycin-mediated potassium transport. *J. Membrane Biol.* **31**:81–102
20. Finkelstein, A. 1964. Carrier model for active transport of ions across a mosaic membrane. *Biophys. J.* **4**:421–440
21. Foster, D.L., Fillingame, R.H. 1979. Energy-transducing H^+-ATPase of *Escherichia coli. J. Biol. Chem.* **254**:8230–8236
22. Frumento, A.S. 1965. The electrical effects of an ionic pump. *J. Theor. Biol.* **9**:253–262
23. Garrahan, P.J., Garay, R.P. 1976. The distinction between sequential and simultaneous models for sodium and potassium transport. *Curr. Top. Membr. Transp.* **8**:29–97
24. Geck, P., Heinz, E. 1976. Coupling in secondary transport. Effect of electrical potentials on the kinetics of ion-linked cotransport. *Biochim. Biophys. Acta* **443**:49–53
25. Geck, P., Pietrzyk, C., Burckhardt, B.-C., Pfeiffer, B., Heinz, E. 1980. Electrically silent cotransport of Na^+, K^+, and Cl^- in Ehrlich cells. *Biochim. Biophys. Acta* **600**:432–447
26. Ginsburg, S., Noble, D. 1976. Use of current-voltage diagrams in locating peak energy barriers in cell membranes. *J. Membrane Biol.* **29**:211–229
27. Glynn, I.M., Karlish, S.J.D. 1975. The sodium pump. *Annu. Rev. Physiol.* **37**:13–55
28. Goffeau, A.L., Slayman, C.W. 1981. The proton translocating ATPase of the fungal plasma membrane. *Biochim. Biophys. Acta (in press)*
29. Gräber, P. 1981. Phosphorylation in chloroplasts: ATP synthesis driven by $\Delta\psi$, by ΔpH, and by $\Delta\bar{\mu}_{H^+}$ of artificial or light-generated origin. *In:* Electrogenic Ion Pumps. C.L. Slayman, editor. Academic Press, New York *(in press)*
30. Gräber, P., Schlodder, E., Witt, H.T. 1977. Control of the rate of ATP synthesis by conformational changes in the chloroplast ATPase induced by the transmembrane electric field. *Proc. Fourth Int. Congr. Photosynth.* D.O. Hall, J. Coombs, and T.W. Goodwin, editors, pp. 197–210. The Biochemical Society (London)
31. Gradmann, D. 1975. Analog circuit of the *Acetabularia* membrane. *J. Membrane Biol.* **25**:183–208

32. Gradmann, D., Hansen, U.-P., Slayman, C.L. 1981. Reaction kinetic analysis of current-voltage relationships for electrogenic pumps in *Neurospora* and *Acetabularia*. *In:* Electrogenic Ion Pumps. C.L. Slayman, editor. Academic Press, New York (*in press*)
33. Hall, J.E., Mead, C.A., Szabo, G. 1973. A barrier model for current flow in lipid bilayer membranes. *J. Membrane Biol.* **11**:75–97
34. Hansen, U.-P., Gradmann, D., Slayman, C.L. 1980. Current-voltage curves and modeling of electrogenic pumps. *Eur. J. Physiol.* **384**:R13, item 52
35. Heinz, E., Geck, P. 1978. The electrical potential difference as a driving force in Na^+-linked cotransport of organic solutes. *In:* Membrane Transport Processes. J.F. Hoffman, editor. Vol. 1, pp. 13–30. Raven Press, New York
36. Heinz, E., Geck, P., Wilbrandt, W. 1972. Coupling in secondary active transport. Activation of transport by cotransport and/or countertransport with the fluxes of other solutes. *Biochim. Biophys. Acta* **255**:442–461
37. Hille, B. 1975. Ionic selectivity, saturation, and block in sodium channels: A four-barrier model. *J. Gen. Physiol.* **66**:535–560
38. Hladky, S.B. 1974. The energy barriers to ion transport by nonactin across thin lipid membranes. *Biochim. Biophys. Acta* **352**:71–85
39. Junge, W. 1970. The critical electric potential difference for photophosphorylation. Its relation to the chemiosmotic hypothesis and to the triggering requirements of the ATPase system. *Eur. J. Biochem.* **14**:582–592
40. Junge, W. 1981. Electrogenic reactions and proton pumping in green plant photosynthesis. *In:* Electrogenic Ion Pumps. C.L. Slayman, editor. Academic Press, New York (*in press*)
41. Kaback, H.R. 1978. Molecular biology and energetics of membrane transport. *J. Cell. Physiol.* **89**:575–594
42. Kaczorowski, G.J., Kaback, H.R. 1979. Mechanisms of lactose translocation in membrane vesicles from *Escherichia coli*. 1. Effect of pH on efflux, exchange, and counterflow. *Biochemistry* **18**:3691–3697
43. Karlish, S.J.D., Yates, D.W., Glynn, I.M. 1978. Conformational transitions between Na^+-bound and K^+-bound forms of $(Na^+ + K^+)$-ATPase, studied with formycin nucleotides. *Biochim. Biophys. Acta* **525**:252–264
44. Kimmich, G.A. 1973. Coupling between Na^+ and sugar transport in small intestine. *Biochim. Biophys. Acta* **300**:31–78
45. Kimmich, G.A., Carter-Su, C. 1978. Membrane potentials and the energetics of intestinal Na^+-dependent transport systems. *Am. J. Physiol.* **235**:C73-C81
46. King, E.L., Altman, C. 1956. A schematic method of deriving the rate laws for enzyme-catalyzed reactions. *J. Phys. Chem.* **60**:1375–1378
47. Kinne, R. 1976. Properties of the glucose transport system in the renal brush border membrane. *Curr. Top. Membr. Transp.* **8**:209–267
48. Komor, E., Schwab, W.G.W., Tanner, W. 1979. The effect of intracellular pH on the rate of hexose uptake in *Chorella*. *Biochim. Biophys. Acta* **555**:524–530
49. Krab. K., Wikström, M. 1980. Proton-pumping cytochrome *c* oxidase. *Biochim. Biophys. Acta* **549**:177–223
50. Kregenow, R.F. 1977. Transport in avian red cells. *In:* Membrane Transport in Red Cells. J.C. Ellory and V.L. Lew, editors. pp. 383–426. Academic Press, New York
51. Kuroda, H., Warncke, J., Sanders, D., Hansen, U.-P., Allen, K.E., Bowman, B.J. 1980. Effects of vanadate on the electrogenic proton pump in *Neurospora*. *In:* Plant Membrane Transport: Current Conceptual Issues. R.M. Spanswick, W.J. Lucas, and J. Dainty, editors. pp. 507–508. Elsevier, New York
52. Lambert, J.D.C., Kerkut, G.A., Walker, R.J. 1974. The electrogenic sodium pump and membrane potential of identified neurones in *Helix aspersa*. *Comp. Biochem. Physiol.* **47A**:897–916
53. Lanyi, J.K., MacDonald, R.E. 1976. Existence of electrogenic hydrogen ion/sodium ion antiport in *Halobacterium halobium* cell envelope vesicles. *Biochemistry* **15**:4608–4613
54. Lanyi, J.K., Silverman, M.P. 1979. Gating effects in *Halobacterium halobium* membrane transport. *J. Biol. Chem.* **254**:4750–4755
55. Läuger, P. 1979. A channel mechanism for electrogenic ion pumps. *Biochim. Biophys. Acta* **552**:143–161
56. Läuger, P., Stark, G. 1970. Kinetics of carrier-mediated ion transport across lipid bilayer membranes. *Biochim. Biophys. Acta* **211**:458–466
57. Lieb, W.R., Stein, W.D. 1974. Testing and characterizing the simple carrier. *Biochim. Biophys. Acta* **373**:178–196
58. Maloney, P.C., Schattschneider, S. 1980. Voltage sensitivity of the proton-translocating adenosine 5'-triphosphatase in *Streptococcus lactis*. *FEBS Lett.* **110**:337–340
59. Mandel, L.J., Curran, P.F. 1973. Response of the frog skin to steady-state voltage clamping. II. The active pathway. *J. Gen. Physiol.* **62**:1–24
60. Markin, V.S., Sokolov, V.S., Boguslavsky, L.I., Jaguzhinsky, L.S. 1975. Nigericin-induced charge transfer across membranes. *J. Membrane Biol.* **25**:23–45
61. Marmor, M.F. 1971. The independence of electrogenic sodium transport and membrane potential in a molluscan neurone. *J. Physiol. (London)* **218**:599–608
62. Mitchell, P. 1966. Chemiosmotic coupling in oxidative and photosynthetic phosphorylation. *Biol. Rev.* **41**:455–502
63. Mitchell, P. 1968. Chemiosmotic Coupling and Energy Transduction. Glynn Research, Bodmin, Cornwall, England
64. Mitchell, P., Moyle, J. 1974. The mechanism of proton translocation in reversible proton-translocating adenosine triphosphatases. *Biochem. Soc. Spec. Publ.* **4**:91–111
65. Moreton, R.B. 1969. An investigation of the electrogenic sodium pump in snail neurones, using the constant field theory. *J. Exp. Biol.* **51**:181–201
66. Morowitz, H.J. 1978. Proton semiconductors and energy transduction in biological systems. *Am. J. Physiol.* **235**:R99-R114
67. Okamoto, H., Sone, N., Hirata, H., Yoshida, M., Kagawa, Y. 1977. Purified proton conductor in proton translocating adenosine triphosphatase of a thermophilic bacterium. *J. Biol. Chem.* **252**:6125–6131
68. Plack, R.H., Rosen, B.P. 1980. Cation/proton antiport systems in *Escherichia coli:* Absence of potassium/proton antiporter in a pH-sensitive mutant. *J. Biol. Chem.* **255**:3824–3825
69. Racker, E. 1978. Mechanisms of ion transport and ATP formation. *In:* Membrane Transport in Biology, Vol. I. Concepts and Models. G. Giebisch, D.C. Tosteson, and H.H. Ussing, editors. pp. 259–299. Springer-Verlag, Berlin
70. Reichert, U., Schmidt, R., Foret, M. 1975. A possible mechanism of energy coupling in purine transport of *Saccharomyces cerevisiae*. *FEBS Lett.* **52**:100–102
71. Requena, J., Mullins, L.J. 1979. Calcium movement in nerve fibres. *Quart. Rev. Biophys.* **12**:371–460
72. Robertson, D.E., Kaczorowski, G.J., Garcia, M.-L., Kaback, H.R. 1980. Active transport in membrane vesicles from *Escherichia coli:* The electrochemical proton gradient alters the distribution of the *Lac* carrier between two different kinetic states. *Biochemistry* **19**:5692–5702
73. Robinson, J.D., Flashner, M.S. 1979. The $(Na^+ + K^+)$-activated ATPase: Enzymatic and transport properties. *Biochim. Biophys. Acta* **549**:145–176
74. Sachs, G., Wallmark, B., Saccomani, G., Rabon, E., Stewart, H.B., DiBona, D.R., Berglindh, T. 1981. The ATP-dependent

component of gastric acid secretion. *In:* Electrogenic Ion Pumps. C.L. Slayman, editor. Academic press, New York (*in press*)
75. Saier, M.H., Jr. 1977. Bacterial phosphoenolpyruvate: Sugar phosphotransferase systems: Structural, functional, and evolutional interrelationships. *Bacteriol. Rev.* **41**:856–871
76. Sanders, D., Hansen, U.-P. 1981. Mechanism of Cl^- transport at the plasma membrane of *Chara corallina*. II. Transinhibition and the determination of H^+/Cl^- binding order from a reaction kinetic model. *J. Membrane Biol.* **58**:139–153
77. Schmitt, W.F., McManus, T.J. 1977. Ouabain-insensitive salt and water movements in duck red cells. I. Kinetics of cation transport under hypertonic conditions. *J. Gen. Physiol.* **70**:59–79
78. Schuldiner, S., Fishkes, H. 1978. Sodium-proton antiport in isolated membrane vesicles of *Escherichia coli*. *Biochemistry* **17**:706–711
79. Schultz, S.G. 1980. Basic Principles of Membrane Transport. 145 pp. Cambridge University Press, Cambridge, England
80. Schultz, S.G., Curran, P.F. 1970. Coupled transport of sodium and organic solutes. *Physiol. Rev.* **50**:637–718
81. Schwab, W.G.W., Komor, E. 1978. A possible mechanistic role of the membrane potential in proton-sugar cotransport of *Chlorella*. *FEBS Lett.* **87**:157–160
82. Segel, I.H. 1975. Enzyme Kinetics. 957 pp. Wiley-Interscience, New York
83. Skou, J.C., Norby, J.G. 1979. Na, K-ATPase: Structure and Kinetics. 549 pp. Academic Press, New York
84. Slayman, C.L. 1974. Proton pumping and generalized energetics of transport: A review. *In:* Membrane Transport in Plants. U. Zimmermann and J. Dainty, editors. pp. 107–119. Springer-Verlag, Berlin
85. Spanswick, R.M. 1972. Evidence for an electrogenic ion pump in *Nitella translucens*. I. The effects of pH, K^+, Na^+, light and temperature on the membrane potential and resistance. *Biochim. Biophys. Acta* **288**:73–89
86. Spanswick, R.M. 1981. The electrogenic pump in the plasma membrane of *Nitella*. *In:* Electrogenic Ion Pumps. C.L. Slayman, editor. Academic Press, New York (*in press*)
87. Stark, G., Benz, R. 1971. The transport of potassium through lipid bilayer membranes by the neutral carriers valinomycin and monactin. *J. Membrane Biol.* **5**:133–153
88. Stark, G., Ketterer, B., Benz, R., Läuger, P. 1971. The rate constants of valinomycin-mediated ion transport through thin lipid membranes. *Biophys. J.* **11**:981–994
89. Stein, W.D., Lieb, W.R. 1973. A necessary simplification of the kinetics of carrier transport. *Isr. J. Chem.* **11**:325–339
90. Stoekenius, W., Lozier, R.H., Bogomolni, R. 1979. Bacteriorhodopsin and the purple membrane of *Halobacteria*. *Biochim. Biophys. Acta* **505**:215–278
91. Tanner, W., Komor, E., Fenzl, F., Decker, M. 1977. Sugar-proton co-transport systems. *In:* Regulation of Cell Membrane Activities in Plants. E. Marre and O. Cifferri, editors. pp. 79–90. Elsevier, Amsterdam
92. Thomas, R.C. 1969. Membrane current and intracellular sodium changes in a snail neurone during extrusion of injected sodium. *J. Physiol.* (*London*) **201**:495–514
93. Thomas, R.C. 1976. Ionic mechanism of the H^+ pump in a snail neurone. *Nature* (*London*) **262**:54–55
94. Thomas, R.C. 1977. The role of bicarbonate, chloride and sodium ions in the regulation of intracellular pH in snail neurones. *J. Physiol.* (*London*) **273**:317–338
95. Wilbrandt, W., Rosenberg, T. 1961. The concept of carrier transport and its corollaries in pharmacology. *Pharmacol. Rev.* **13**:109–183

Received 16 January 1981